Numerical and experimental study of the vortex length in a gas cyclone

Ellinor Arguilla Svensen
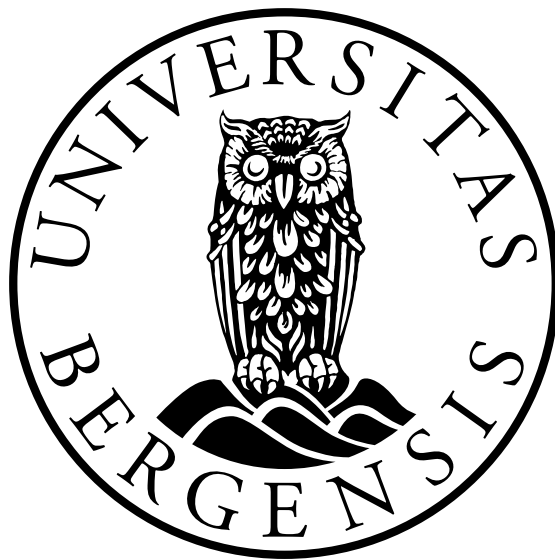
Master Thesis Process Technology

Department of Physics and Technology
University of Bergen

September 2012

Acknowledgements

I would like to thank my supervisor Professor Alex C. Hoffmann for his guidance throughout this thesis. I would also like to thank him for the inspiring conversations and valuable support. I would also like to thank my fellow students, both in the Process Technology group and the Atomic Physics group whom I shared the office with, for good discussions and appreciative breaks during the work. The student way of life would not have been the same without you. A special thank to Dr. Gleb Pisarev and Torill Rødland for cooperation with the experimental work.

I am also grateful for all the help I have gotten from my dad, Andreas Christiansen, not only with this thesis but through my whole life and eduction. Thank you for the all the guidance, and also the help with reviewing this thesis.

I would also thank my family and friends for all their help, tolerance and being there when needed.

To the love of my life, my husband Øyvind. I could not have done this without you. You have been a tremendous support for me. Thank you for the explanatory conversations, the moral support and for all the encouragement you have given me.

Contents

List of Figures

Chapter 1

Introduction

Cyclones are widely used in many kinds of industry as a separation method. The denser phase is separated from the lighter due to centrifugal forces, for example particles can be separated from gas, or water from oil.

The two most common cyclones are the cylinder-on-cone cyclones with tangential inlet and swirl tubes, which is normally cylindrical with swirl vanes at the inlet, as shown in figure 1.1. There are design variations within these two types, which are discussed in section 2.1.1. The principle for both types are the same; gas enters by the inlet at the top, moves in a swirling motion downwards, the particles, or denser phase, are separated out and exits at the bottom. If the cleaned fluid exits at the tube at the top, it is called a reversed-flow cyclone.

Regulations for particle pollution have become increasingly strict because of the environmental issues. This causes the process industry to focus more on particle emission, and is one important reason for capturing particles in process. Other reasons for maintaining good separation are economical ones, like re-using the particle in the process (for example catalytic particles), and after further processing it can sometimes be included with a product and sold to the customer.

1.1   History of cyclones

In 1885, the first patent of a cyclone was made in the United State of America, with the Knickerbocker Company [1]. It had a very different design than cyclones today, for instance the dust exited on the side and not at the bottom, but the principle was the same as today; using centrifugal forces, instead of gravity, as in a sedimentation tank, to separate dust from gas, saving time and space.

Others followed and by early 18th century the cyclones began to look more like todays design. The first cyclones were used to collect dust particles from farmers mills, mostly processed grain and various wooden products. But today one may find cyclones in all kinds of industry, where particles are cleaned from gas. They are widely used because of their simple design, and because they can be easily implemented in exciting systems.

(a) Cylinder-on-cone cyclone   (b) Swirl tube
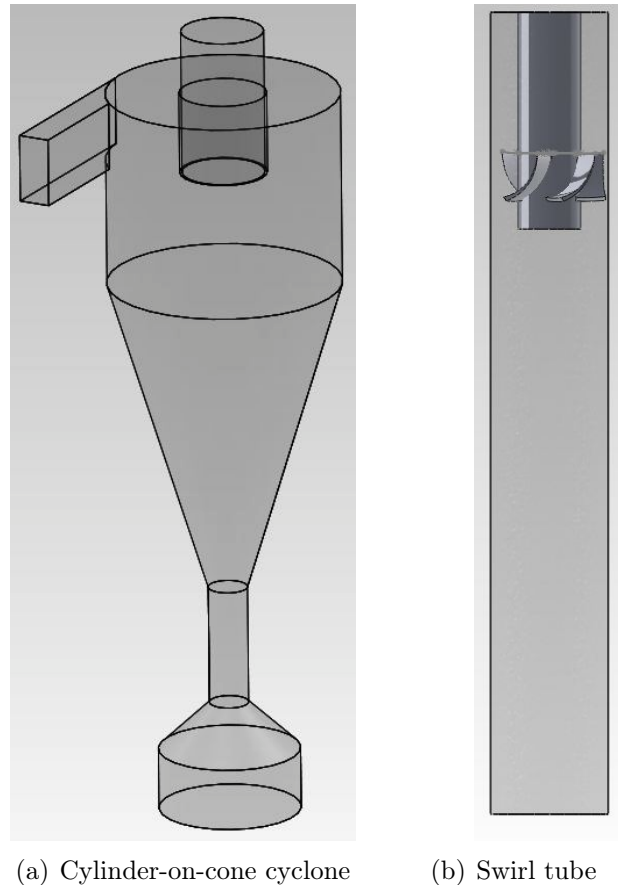
Figure 1.1: The two main types of cyclone formation, cylinder-on-cone and swirl tube

1.2   Areas of application

There are many areas of utilization for cyclones. Some examples of this are: power stations, food processing plants, chemical industries, metallurgical industries and dust sampling equipments. Even in central vacuum cleaners, cyclones are used.

Cyclones can effectively separate two-phase mixtures, where the denser phase is separated out. For instance water droplets from steam generators and coolers can be removed, and entrained oil and hydrocarbon droplets in water from process industry.

The advantages over other separation equipment, like filters, scrubbers and settlers which often requires larger space and/or has exchangeable parts that need maintenance, are that the cyclone is only driven by a pump, and has no moving parts. This makes it easy to maintain and with a comprehensive area of utilization.

1.3   How a cyclone works

As mentioned at the beginning of this chapter, particles or a denser phase are separated from lighter fluids because of the swirling motion in the cyclone. The flow changes from linear to a swirling flow at the inlet, for example a tangential inlet or swirl vanes (for more details on inlet see chapter 2.1.1).

The gas flow swirls downward in the outer vortex, turns at some point and flows up again in the center, the inner vortex [1]. If the cyclone is positioned vertically, the

gravity force will help the separation of particles in the flow. This, however, is not the critical force, the downward flow is. A more detailed discussion of the flow pattern can be found in section 2.1.2.

In the performance studies, a great deal of attention has been paid to the impact of the velocity, viscosity, density of particles, particle concentration and shape and size distribution [1]. Because of this there are specialized designs for different operating conditions. The main focus has been on separation efficiency and pressure drop., since it is wanted to have highest efficiency and lowest pressure drop in a cyclone.

1.3.1 The phenomenon "End of the vortex"

During the last years, some attention has also been paid to the effect of the length of the vortex inside the cyclone, since the length of the vortex is the effective length of the cyclone. Normally in a reversed flow cyclone, the vortex flow extend to the bottom of the cyclone before it turns and goes out through the vortex finder. This is called a centralized vortex, and has the best separation efficiency; the whole cyclone body is utilized and all pressure loss and particle separation takes place in this area. But in some cases the vortex ends on the cyclone wall instead, there it remains at a stable position and rotates around the cyclone body attached to the wall. This phenomenon is a flow instability, and is called "the end of the vortex", EoV, and can be seen in figure 1.2.

a) Centralized vortex   b) End of vortex phenomena
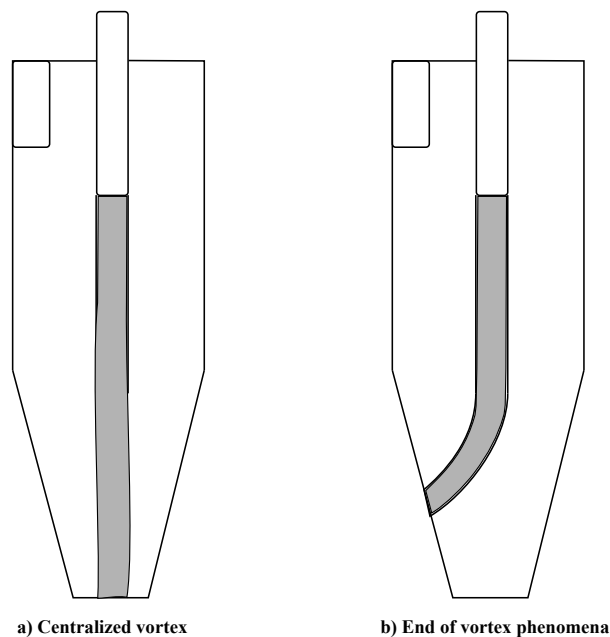
Figure 1.2: A centralized vortex in a cyclone, and the end of the vortex phenomenon: The vortex reach its turning point at the cyclone wall

The end of the vortex is often reported as a ring pattern in the dust on the cyclone wall [2][3][4]. By using visualization techniques that does not influence the flow pattern, the dust ring has been explained as the vortex core bending to the wall and rotating at a stable position with a relatively constant frequency [5]. Pressure transducer can also be used to measure the position of the vortex end, since the pressure is lower in the vortex core than in the rest of the flow.

There has not been done many extensive studies on the length of the vortex, called the natural vortex length, and which parameters influence this. Cyclone models indicate, and it is natural to think that, if the cyclone is longer, the vortex, and separation space, will be longer, and to some extent this is true. But it can not be made arbitrary long for a larger separation space. At some point, the vortex will bend to the wall.

The vortex core is where the separation takes place, and by remaining on the wall it can for example cause erosion, clogging and cause re-capturing collected particles in the gas flow. It is therefor crucial to know how the phenomenon acts. This is explained later in this thesis.

When studying the vortex flow, the disadvantage with gas is that in most cases it is invisible. To make it visible, some substance, like smoke or particles, has to be added, and this may influence the flow pattern. Previous models for the length are not consistent with each other and only include a few geometrical parameters[6][7][2][8].

It is also known that roughness influences the vortex length [9][10], but this is not a design parameter rather than an abrasion (as the cyclones are normally made as smooth as possible), so it is natural that this is not a part of the model for the length. But still it is important to study the impact on the vortex.

The end of the vortex phenomenon does not only act in cyclones, a study performed on vortex diodes showed the same behavior of the vortex core [11].

1.4 Computational Fluid Dynamics

The use of computational efforts to model physics has expanded the latest years, and has made simulations of flow possible. Solving the Navier-Stokes equations for fluid mechanics is in most practical cases not possible. Methods for numerical solutions where made over a century ago, but did not have much practical use before computers were used [12]. Computational Fluid Dynamics, or CFD, has advanced greatly as computer technology has advanced.

In the 1950s, there were built computers that could do only a few hundred operations per second. Todays computers that have up to 10^{12} floating point operations per second, and development in computer technology has far from stopped. The potential in CFD is enormous, in many fields of engineering, like process, chemical, civil and environmental.

The Navier-Stokes equations are partial differential equations that describe flows and related phenomena. A good textbook in fluid dymanics is "Transport phenomena" by Bird et. al (2007) [13]. For these equations to be solved, a discretization method is used [12]. Both time and space are discretized and the equations are approximated and solved by a computer.

CFD is now widely used for simulations of different types of flow. In this thesis the commercial software Star CCM+ will be used.

1.5 Background

The multiphase-system group in the Process technology department at the institute of Physics and technology at the University of Bergen has an ongoing project in collaboration with the University in Utrecht. This project focuses on modeling and analyzing

the phenomenon "end of the vortex" which appears in cyclones. The project is funded by the Norwegian Research Council.

This project has been running at the University of Bergen since 2010. PhD. Gleb Pisarev [14] studied the effect of size of the dust collector, also called dust hopper, and found that if the hopper was not deep enough, the vortex ended in the bottom of the hopper. He also found that the position of the vortex end was independent of inlet gas velocity. He successfully modeled swirl tubes using CFD. McS. Vidar Gjerde [15] did a mostly experimental study of the vortex end in swirl tubes of different lengths, and pressure measurements using transducers connected to the cyclone wall using almost the same experimental rig as in this thesis. McS. Torill Rødland [16] studied the effect of surface roughness, both experimentally and by simulations of swirl tubes. She found that higher roughness decreased the vortex length.

1.5.1   Goal of this thesis

The goal of this thesis is to make a new model for the vortex length, including more parameters than the previous ones that are expected to influence the vortex length. By using CFD simulations, many different geometries may be tested without having several different physical units. A factorial scheme can then be set up, to test which geometrical and operational factors effect the length of the vortex within a certain range. This model can then be used to decide operating conditions and design the cyclone for best performance according to natural vortex length. The thesis will build on previous work done in the group in the University of Bergen.

In this thesis, the end of the vortex phenomenon in swirl tubes was studied experimentally, to show the existence of the end of the vortex phenomena and the influence of cyclone length. CFD models were built to model the flow in cylinder-on-cone cyclones and compared with previous experiments. The importance of near wall modeling was studied, the length of the cyclones dependence of geometrical parameters and inlet velocity, and the effect of roughness in cylinder-on-cone cyclones.

1.6   Outline of the thesis

The thesis is organized in the following chapters:

- In Chapter 2: Theory, the basic concepts and fluid dynamics in cyclones is discussed. Theory about CFD in general and planning of experiments is also given.

- In Chapter 3: Literature survey, a summary is given of pervious research done concerning the length of the vortex in a cyclone and CFD on cyclones in general.

- In Chapter 4: Experimental, the experimental setup is presented, the use of equipment and measurement methods.

- In Chapter 5: Development of computational techniques and design of numerical experiments, gives a description of techniques used in the CFD model and an introduction to planning of experiments with a factorial scheme.

- Chapter 6: Computational simulations, is dedicated to the CFD simulations and how the model was built.

- Chapter 7: Results and discussion, gives the results of both the experimental and the computational work and a discussion of the results.

- In Chapter 8: Conclusion and outlook, the thesis is concluded and suggestions for further work are given.

It is expected that the reader has some basic knowledge in physics and mathematics. Some knowledge about process technology is also an advantage.

Chapter 2

Theory

To better understand the experiments and simulations done in this thesis, background material for cyclone theory, computational fluid dynamics and design of experiments will be given.

2.1 Cyclones

2.1.1 Design

The two main types of cyclones, cylinder-on-cone cyclones and swirl tubes [1], is shown in figure 1.1.

The swirl tube is cylindrical all the way down, while the cylinder-on-cone cyclone has, as the name implies, a cylindrical section on top of conical section. This thesis will mainly discuss cylinder-on-cone types, except the experimental work that will focus on swirl tubes.

There is a wide variety of designs for cylinder-on-cone cyclones with tangential intel. The most common ones are given in table 2.1. To make them comparable, the dimensions are recalculated so they have an inlet area of 0.01 m^2 (same volumetric flow rate). Each type is designed for a special type of use. The geometry parts of a cyclone can be seen in figure 2.1. Not all cyclones have tangential inlet, but this is the most common.
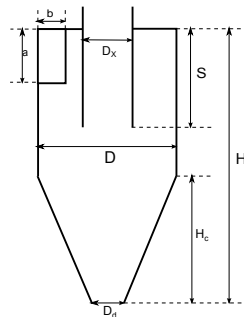
Figure 2.1: Significant cyclone geometry parts. D_x is the diameter of the vortex finder (gas outlet), ab is the inlet area, S is the distance from the cyclone top to the bottom of the vortex finder, D is the diameter of the cyclone body, H_c is the height of the conical part, H is the total height and D_d is the diameter of the dust outlet. Dimensions for the most common cyclones can be seen in table 2.1, [1].

Table 2.1: Cyclone geometries [1]

Name	D	D_x	S	H	$H-H_c$	a	b	D_d
Muschelknautz E	680	170	311	934	173	173	58	228
Muschelknautz D	357	119	318	863	262	187	54	195
Storch 4	260	117	176	1616	909	260	38	91
Storch 3	192	107	200	821	462	167	60	92
Storch 2	225	108	239	1097	464	188	53	84
Storch 1	365	123	142	1943	548	100	100	64
Tengbergen C	337	112	145	930	187	100	100	112
Tengbergen B	210	112	224	604	324	179	56	112
Tengbergen A	277	112	157	647	180	135	74	202
TSN-11	348	136	242	959	219	184	54	154
TSN-15	266	158	350	1124	589	166	60	119
Stairmand HE	316	158	158	1265	474	158	63	119
Stairmand HF	190	141	165	755	283	141	71	71
Van Tongeren AC	325	100	325	1231	436	149	67	130
Vibco	286	111	124	720	228	111	90	66
Lapple GP	283	141	177	1131	566	141	71	71

Scale drawings of the cyclones in table 2.1 can bee seen in figure 2.2, all the cyclones listed can be seen from left to right. As one can see there is a wide variety . The most common one is the Staimand High Efficiency (Stairmand HE).
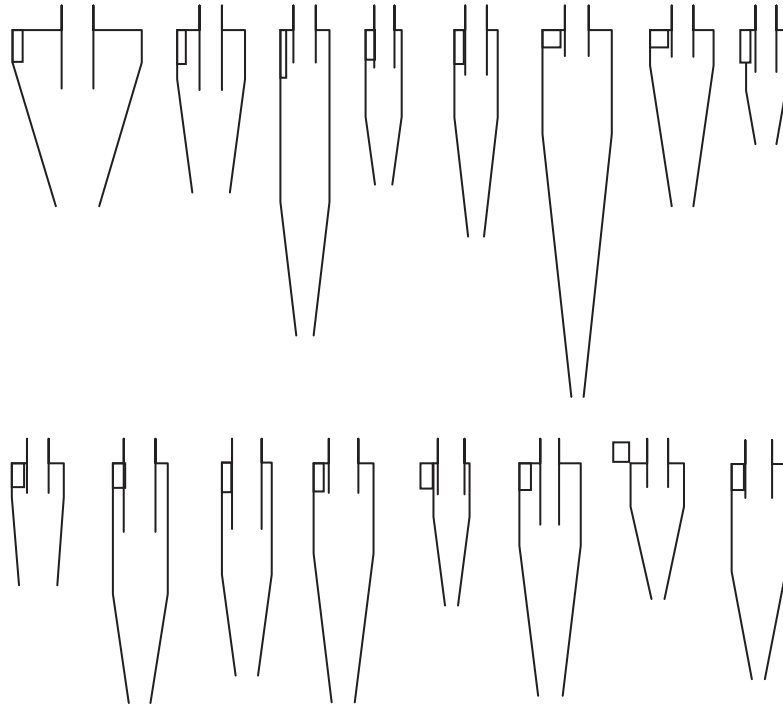
Figure 2.2: Scale drawings of the different cyclone geomteries in table 2.1, [1].

Inlet

On a cylinder-on-cone cyclone the inlet area is often rectangular shaped [1]. There are some cyclones with circular cross section, but this is not widely used. The design parameters for a rectangular inlet are length (a) and width (b). For better performance,

the width should be as narrow as possible (for the given operating flow rate), thus the particles enter closer to the wall (see section 2.1.2) [17].

There are different types of inlets. The pipe-inlet, is a circular pipe as an inlet. With this a round-to-rectangular inlet transition needs to be made also. The most common one are the rectangular slotted inlet, this is also called a tangential inlet. The scroll or volute inlet, is a "wrap-around"-type, where the inlet is on the outside of the cyclone body. This is the preferred type with large vortex finder diameters, because the gas flow will not impact the wall of the vortex finder. The axial type of inlet is most often swirl vanes, these will be described later on in the section concerning swirl tubes.

It has also been done some research on a double inlet configuration. Zhao et al (2006) [18] found that using a double inlet improved the symmetry of the vortex, and thus improve the separation efficiency.

The most common inlets, together with the double inlet can be seen in figure 2.3. The inlet of the swirl tube can be seen in figure 2.6. There are different ways to bound the inlet tube with the cyclone body.
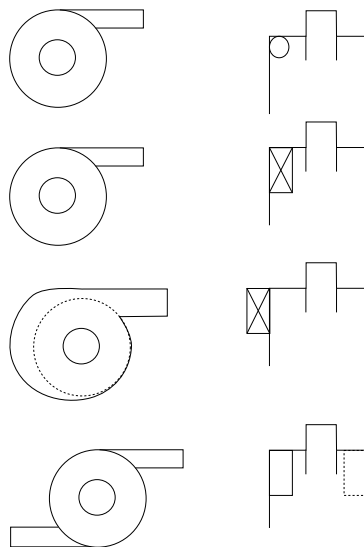
Figure 2.3: The three most common cyclone inlets; the circular, rectangular, volute (wrap-around inlet), and a new type: the double inlet. [1], [18].

Gas outlet (vortexfinder)

The vortex finder, or gas outlet, is normally a cylindrical tube inserted in the cyclone body to approximately where the inlet duct ends [1]. This is called a reversed-flow cyclone. The diameter, length and insertion depth can be varied, but also some geometry variations like a "top" or different tailpieces to the tube is utilized. On figure 2.1 the vortex finder is situated on the top of the cyclone body, and the diameter of the vortex finder tube is marked as D_x. The gas can also exit at the bottom, a flow-through cyclone, but these cyclones are almost always purely cylindrical.

Dust outlet

It is important to carefully design the dust outlet in order to prevent collected dust being caught in the vortex and re-enter the cyclone [1]. A cylindrical tube can be placed under

the cyclone body, connecting the body and the dust collection chamber (dust hopper), which helps stabilize the vortex. If the tube is made longer, it stabilizes the vortex, but causes some pressure drop [19].

The depth of the dust hopper is also important. Pisarev et. al (2010) [14] did computational simulations of different depths of dust hoppers, as seen in figure 2.4. He found that if the dust hopper is made too narrow, the vortex will end in the bottom of the bin.
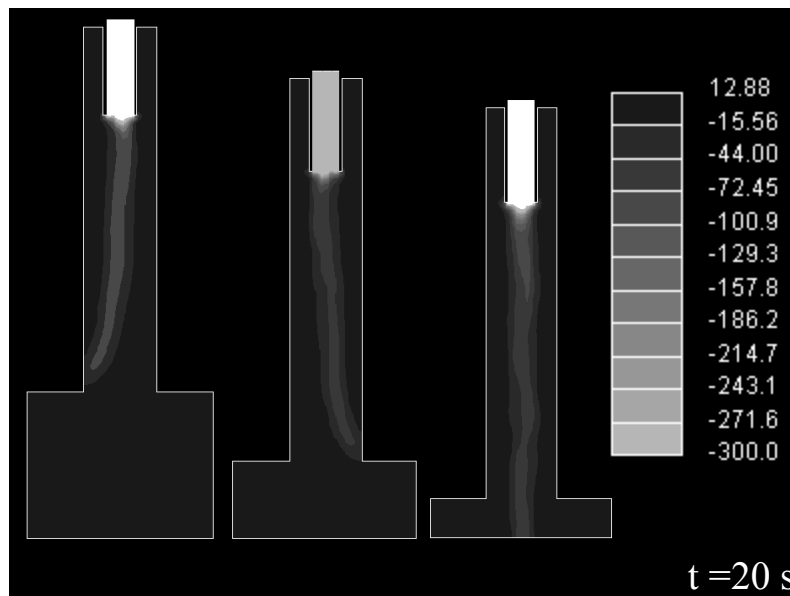
Figure 2.4: Static pressure plots for cyclones with dust hopper of different depths and the effect on the vortex length, results of Pisarev (2010), [14].

A dipleg (a cylindrical tube) can also be used between the cyclone body and the dust hopper to prevent the vortex to end in the dust hopper. In most cases it would end in the dipleg instead. This was found in the work of both Gil et. al [4] and Hoffmann et. al [3].

Conical section

In cyclones with a conical section one can have wide angle or narrow angled cyclones 2.5, and everything in between. The variation is the length of the cylindrical section (on top) and the conical section. The total body length can remain constant, and the difference is the length of the cylindrical to the conical section.

Swirl tubes

Swirl tubes consist of a cylindrical body, a vortex finder (like on a cylinder-on-cone cyclone) and an axial inlet positioned around the vortex finder. The characteristic swirl vanes angles the gas flow and the vortex forms beneath the vanes. The vanes are shown in figure 2.6. The whole swirl tube can be seen in figure 1.1(b)

The exit angle, β, has a recommended angle of 15-30 % [1]. By decreasing β the swirl intensity is increased along with the separation efficiency and pressure drop. Although the angle can not be made to narrow due to boundary layer separation and generation of

(a) wide angle   (b) narrow angle
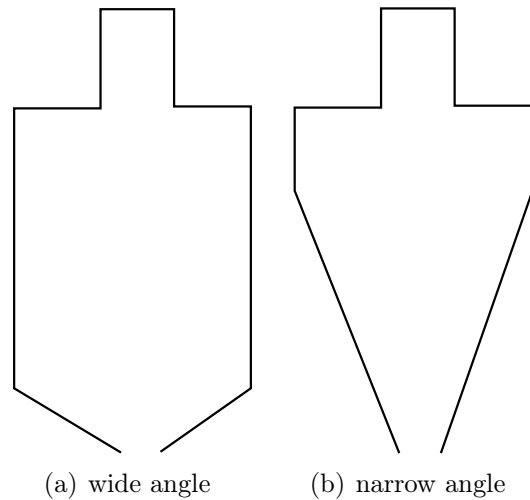
Figure 2.5: Wide angle and narrow angle conical section
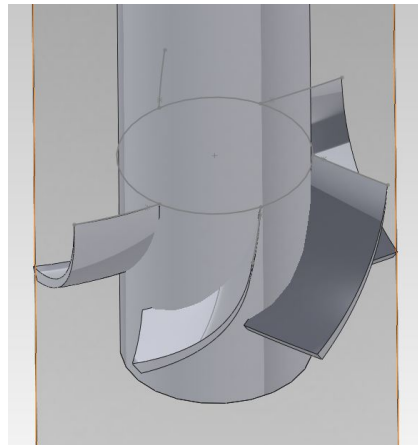
Figure 2.6: Swirl vanes in the inlet of the swirl tune. The vortex forms under the vanes.

turbulence in the vane pack itself. The shape of the vanes is also important. 2-D vanes only bend in one direction, and 3-D vanes are twisted.

Like for a cylinder-on-cone cyclone the the performance is influenced by the length of the vortex, but the effect seems less invasive for a swirl tube. If the vortex end is on the wall and not the bottom of the tube, theres is a shortening in the separation space, but this is the main effect [1]. In cylcinder-on-cone cyclones erosion and clogging is also a huge effect.

2.1.2   Flow pattern

Turbulent flow

The flow in a cyclone is dominated by turbulent flow. Turbulence differs from laminar flow by the eddying motion (local swirling with often very intense vorticiy) [20].

A dimensionless number, the Reynolds number, is used to describe if a flow is laminar or turbulent.

$$Re = \frac{\rho v D}{\mu} = \frac{Dv}{\nu} \tag{2.1}$$

Where v is the velocity, μ is the dynamic viscosity, ρ is the density, ν is the kinematic viscosity and D is some characteristic dimension (for example diameter of tube) of the system. Low Re corresponds to a laminar flow (for flow in pipe Re< 2100), and high Re corresponds to a turbulent flow (Re> 4000 for pipe flow), and a transition area in between [21].

In a laminar flow the fluid flows in parallel in straight lines, when the flow is turbulent there is erratical moving in form of cross-currents and eddies. There are larger eddies, which carries most of the energy and cascades the energy to the smaller eddies, and the smallest eddies dissipates to heat due to viscosity of the fluid. The range of scales is a continuous spectrum, but can be quantified in terms of eddies or wavelengths. An eddy is the local swirling motion.

The turbulence flow pattern acts as an cascade of turbulent eddies [20], there is the larger energy-containing eddies that tranfser energy to the smaller eddies as the turbulence disintergrate, and the smallest one dissipate into heat.

The rate at which the smallest eddies dissipate to heat, should be the same as the larger eddies transfer energy to the smaller eddies. Therefor the movement of the smallest scales is dependent on the rate of the energy passage, ϵ = -dk/dt, and the kinematic viscosity, ν. This is given in the universal equilibrium theory of Kolmogorov (1941) [22] as a length (η), time (τ) and velocity (v) scale for the smallest eddies in a turbulent flows.

Length scale:

$$\eta = \left(\frac{\nu^3}{\epsilon}\right)^{\frac{1}{4}} \tag{2.2}$$

Time scale:

$$\tau = \left(\frac{\nu}{\epsilon}\right)^{\frac{1}{2}} \tag{2.3}$$

Velocity scale:

$$v = (\nu\epsilon)^{\frac{1}{4}} \tag{2.4}$$

The smallest eddies are in the side of 10-100 μm. Eddies that are smaller than this dissipates due to viscous shear [21].

The largest eddies, l_e are the ones the contributes the most to the turbulent flow [23]. But since the flow is dissipative, it is also dependent of ϵ and v. The largest scales are much larger that the ones of Kolmogorov length scale. Between the part where the large energy-containing eddies is most important, and the part of the smallest eddies dissipate to heat due to viscosity, there is a range of eddy sizes where the energy cascade is independent of the statistics of the large eddies and the effect of the viscosity. This is called the inertial subrange, and the energy is here transferred by inertial effects.

A typical energy spectrum for a turbulent flow is shown in 2.7. Since the eddies act as a cascade, transferring energy to the smaller eddies, it is common to represent the energy as a continuous specter and not discrete values [23].

In a pipe of diameter d, the different sizes of eddies can be calculated from the Reynolds number [22].

The largest eddies:
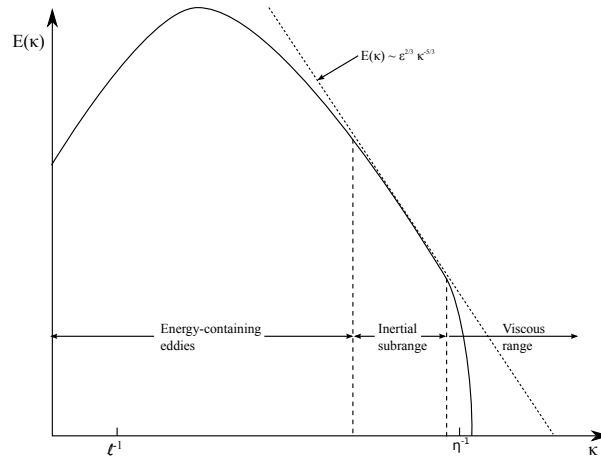
Figure 2.7: Energy spectrum in turbulent flow

$$l_e = 0.05 d Re^{-\frac{1}{8}} \tag{2.5}$$

The kolmogorov length scale:

$$\eta = 4 d Re^{-0.78} \tag{2.6}$$

The most dissipative eddies are about 5η:

$$l_d = 20 d Re^{-0.78} \tag{2.7}$$

In a wall bounded flow (in a pipe or on a solid body) the flow pattern changes near the wall. There is a turbulent core in the middle, and different boundary layers closest to the wall which is influenced by the solid boundary, which is called the Law of the Wall [20]. The viscous sublayer is the first boundary layer and the next is called the log layer (or buffer layer). In the viscous sublayer, which is the first thin, laminar layer between the interface and the bulk of the fluid the velocity gradient is constant, there is some eddying movement, but not much compared to the turbulent region [21]. The buffer layer is the transition between laminar outer layer and turbulent core.

The velocity distribution is often given as dimensionless parameters.

Friction velocity:

$$u^* = \bar{V} \sqrt{\frac{f}{2}} = \sqrt{\frac{\tau_w}{\rho}} \tag{2.8}$$

Velocity quotient:

$$u^+ = \frac{u}{u^*} \tag{2.9}$$

Dimensionless distance:

$$y^+ = \frac{y}{\mu} \sqrt{\tau_w \rho} \tag{2.10}$$

where y is the distance from the wall.

A typical profile the dimensionless distance in the different layers, see figure 2.9
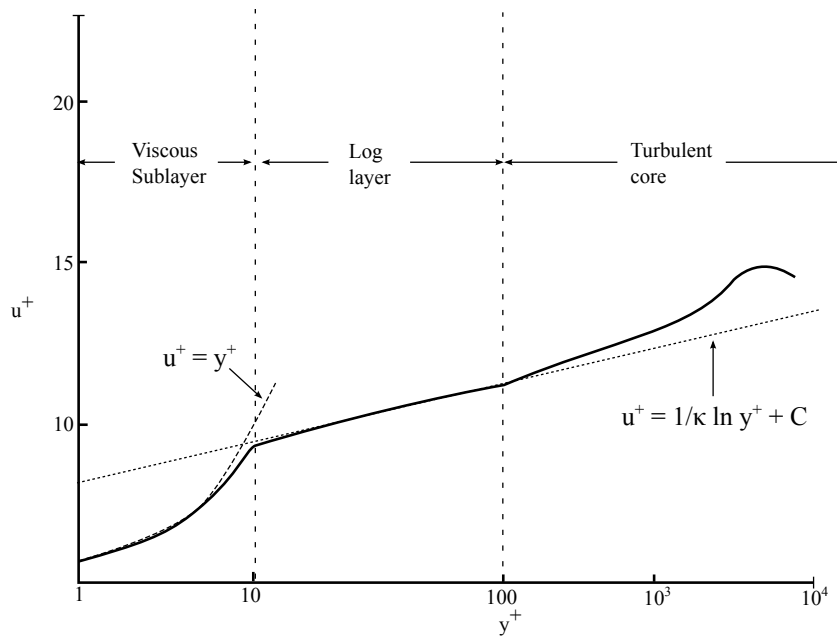
Figure 2.8: The velocity distribution in the different boundary layers in a turbulent flow. Made from [20].

Flow in a cyclone

In a cyclone, a swirling motion is created at the inlet, either by tangentially injecting the air or by swirl vanes in a swirl tube (see section 2.1.1 on different inlet designs). The gas flowing downwards moves in the outer vortex, and up again in the inner vortex and out the vortex finder [1].
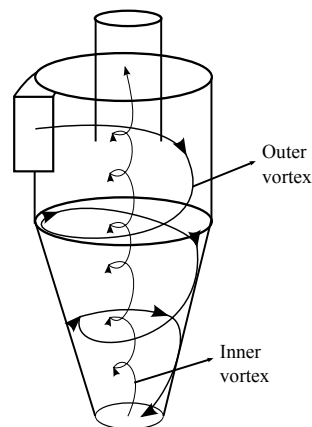
Figure 2.9: The flow pattern in a cyclone. The downward directed outer vortex and the upward directed inner vortex. Made from [1].

Axial velocity distribution from the center to the wall can be seen in figure 2.10(a). From this one can see the downwards directed outer flow, and the upwards directed inner flow. There is a radial flow from the outer vortex to the inner, under the vortex finder.

The radial tangential velocity distribution can be seen in figure 2.10(b) Two types of ideal swirls can be defined; a forced vortex flow (like a rotating solid body), and a free vortex flow (frictionless fluid), the tangential velocity distribution of a real swirling flow would be something in between. This is close to what is called a Rankine vortex.

(a) Axial velocity distribituion

(b) Tangential velocity distribution
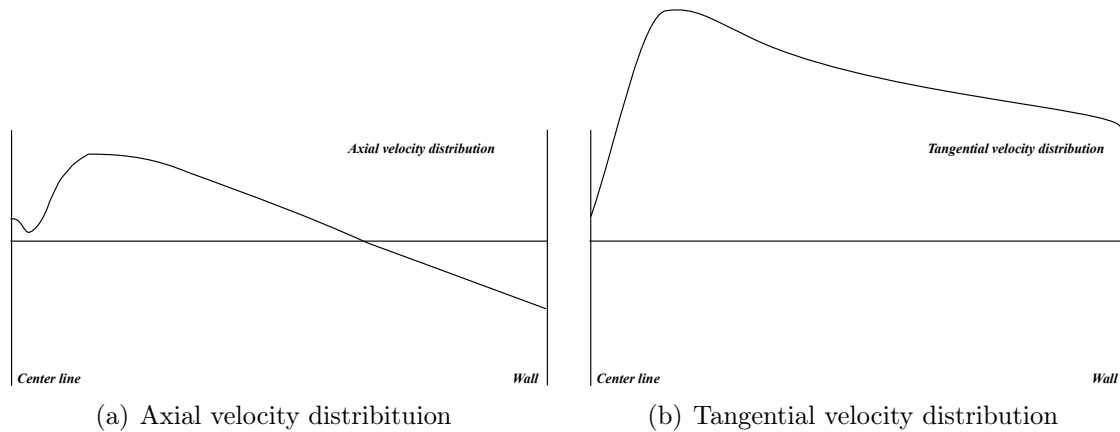
Figure 2.10: Axial and tangential velocity distributions in a cyclone, from the center to the wall

The tangential velocity in forced vortex flow, a flow with infinite viscosity, can be described by:

$$v_\theta = \Omega r \tag{2.11}$$

where Ω is the angular velocity and r is the radius.

The other ideal flow, is the another extreme, the frictionless fluid flow, with no viscosity. The tangential velocity in frictionless flow is given by:

$$v_\theta = \frac{C}{r} \tag{2.12}$$

where C is a constant.

A real vortex flow would be close the solid body rotation near the core, and the loss free rotation in the surrounding, this can be seen in figure 2.11.
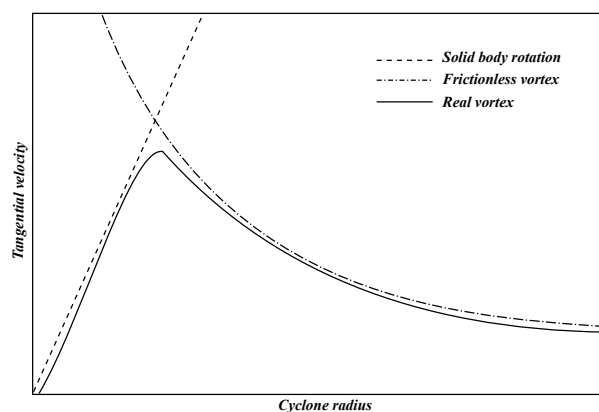
Figure 2.11: The tangential velocity how a solid body rotation and a loss free vortex flow would be, and how the real vortex flow acts from center along the radius. Made from [1]

The tangential velocity is low in the boundary layers near the cyclone wall. This causes a net inwardly directed flows of the gas situated closest to the wall (on the cyclone roof and conical wall), a secondary flow. The inward force is being balanced by frictional drag forced with the wall and bulk flow. See figure 2.12.
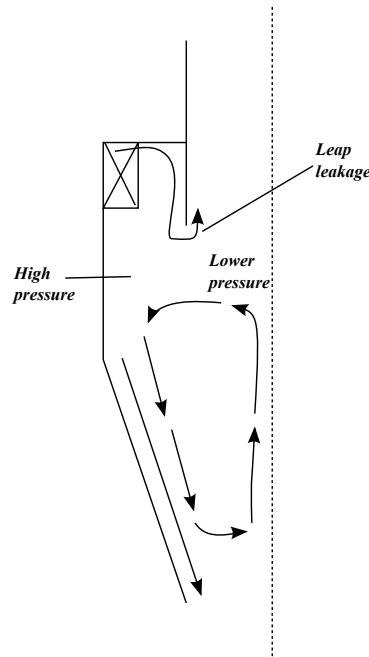
Figure 2.12: Secondary flow in a cyclone

The particle flows in to the cyclone with the gas. The separation starts at the same time as the swirling motion[1]. Some of the particles will be separated and some will follow the gas flow out of the cyclone again. This is further explained in the section about separation efficiency, section 2.1.6. Partical movement is not easily studied experimentally, but it can be studied with CFD simulations. There has been done a lot of research on this, but it will not be treated in this thesis.

Forces

A centrifugal force is developed in the vortex, this cause the particles to be "thrown" to the wall, and because of the gravity force falls down along the side and is collected at the bottom. The centrifugal force acts radially, and the gravitational force is acting vertically [21]. The gravitational is quite weak compared to the centrifugal force, it is the centrifugal force that mainly cause the downward stream and the particles to separate, but it is "helped" by the gravitational force. To better describe the swirling flow, a fluid element can be considered, and then look at the forces acting on it. See figure 2.13.

Centrifugal force:

$$F_c = \frac{mu_{tan}^2}{r} \tag{2.13}$$

Gravitational force:

$$F_g = mg \tag{2.14}$$

The centripetal acceleration acts towards the center, and an equal force (centrifugal force) acts in the opposite direction [1].

In the cyclone, near the wall, the pressure gradient is very strong through the boundary layer and is an important cause of the secondary flow mentioned in previous section.
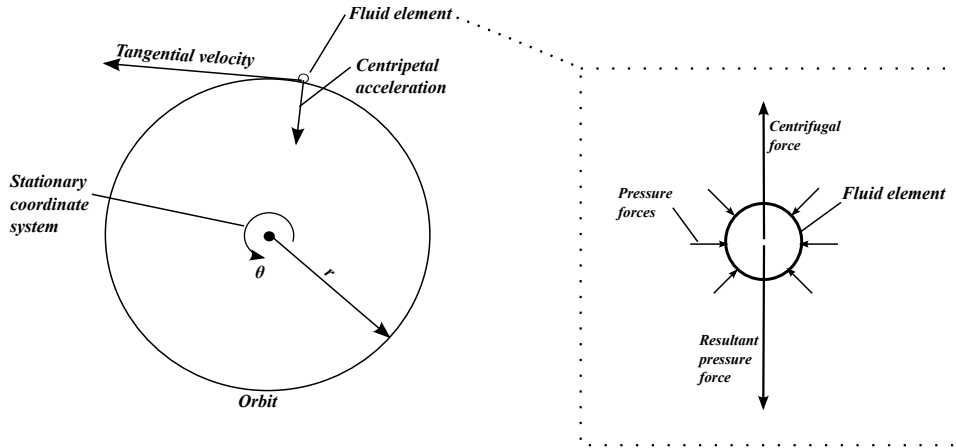
Figure 2.13: A fluid element in a swirling flow. Where r is the radius of the orbit the element moves at, and θ is the angular velocity in a stationary coordinate system. The centrifugal force exerts an equal and opposite force. Made from [1]

Because of the high pressure in the outer region, and low pressure in the core, it is important to have the walls as smooth as possible. Disturbances can cause the fluid to deflect radially inward, and separated particles can be caught in the flow again.

2.1.3 Pressure distribution

Bernoullis equation for frictionless fluid with constant density:

$$\frac{p}{\rho} + gh + \frac{1}{2}v^2 = \text{ constant along a streamline} \tag{2.15}$$

A friction term could be added, but the Bernoulli equation as it is, is a good estimate for the outer vortex flow [1].

p is the static pressure and $\frac{1}{2}\rho v^2$ is the dynamic pressure. From figure 2.14 the pressure distribution of static and dynamic pressure can be seen. As excepted the both the static and the dynamic pressure is almost constant in outer vortex part, and then decreases drastically towards the center. The same tendency is seen inside the vortex finder, which is also expected since the vortex is also present here.
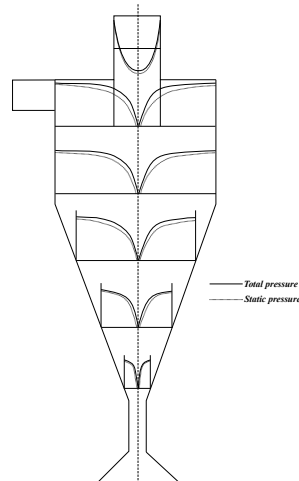
Figure 2.14: Static and total pressure profiles in a cyclone

The vortex flow is not a symmetrical flow as the sketch of the pressure profile might imply. The lowest pressure is in the center of the vortex core, so if the vortex is not centralized the pressure distribution would look different.

Pressure distributions obtained from CFD simulations can be seen in figure 2.15. There you can see both a cross section of cyclone body, and the pressure distribution where the EoV phenomenon is present.

(a) Cross section   (b) EoV
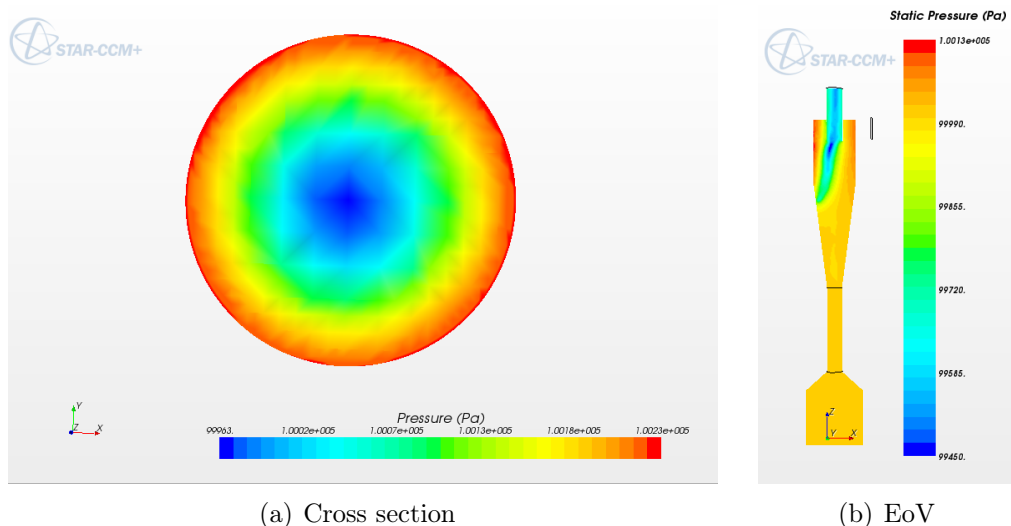
Figure 2.15: The pressure distribution seen in a cross section of the cyclone body and with EoV present

2.1.4 Pressure drop

There are mainly three contributions that cause pressure drop in a cyclone:

- Losses around the inlet

- Losses in the cyclone body

- Losses around the vortex finder

Losses around the inlet, especially for cyclones with tangential inlets, are often negligible. For swirl tubes there can be some losses, but the vanes are normally aerodynamically shaped and therefor the losses are small. Cyclone body losses are somewhat higher, but the main significance is the swirl intensity. The more frictional losses at the walls, the less intensive swirl. The largest losses can be found in the vortex finder.

The pressure drop over a cyclone, δP, is close to proportional to the square of the volumetric flow rate (like all processing equipment with turbulent flow).

A dimension less characteristic is given as the Euler number:

$$Eu := \frac{\Delta p}{\frac{1}{2}\rho \widetilde{v_z}^2} \qquad (2.16)$$

where $\widetilde{v_z}^2$ is the mean axial velocity in the cyclone body.

2.1.5 Flow rate

The volumetric flow rate in m^3/h is given as:

$$Q = v_{in} \cdot A_i \cdot 3600 \tag{2.17}$$

where v$_{in}$ is the inlet velocity and A$_i$ is the inlet cross section area (ab).

Gjerde [15] did experiments on the flow rate needed for vortex to centralize. He found that a higher flow rate would cause centralization.

2.1.6 Efficiency

The efficiency of a cyclone gives the separation characteristics in terms of particles separated from the gas.

Overall separation efficiency:

$$\eta = \frac{M_c}{M_f} = \frac{M_c}{M_c + M_e} \tag{2.18}$$

where M$_c$ is the captured particles and M$_e$ is the emitted. The overall efficiency gives the fraction of particles collected in the underflow.

A more descriptive manner of giving the efficiency, is with a grade-efficiency curve (GEC) [1]. The GEC shows the separation efficiency for each particle size in a given range. The size that is separated with an efficiency of 50% is called the "cut size".

Mass balance for dust with particles less than a size x:

$$F_f(x) = \eta F_c(x) + (1 - \eta) F_e(x) \tag{2.19}$$

The grade-efficiency is the fraction of the particles in the feed collected in the cyclone with a diameter in the range $\left[x - \frac{1}{2}dx, x + \frac{1}{2}dx\right]$. By inserting equation 2.18 and 2.19 one get for the grade-efficiency

$$\eta(x) = \frac{M_c f_c(x)dx}{M_f f_f(x)dx} = 1 - (1 - \eta)\frac{dF_e(x)}{dF_f(x)} \tag{2.20}$$

An example of a GEC can be seen in figure 2.16
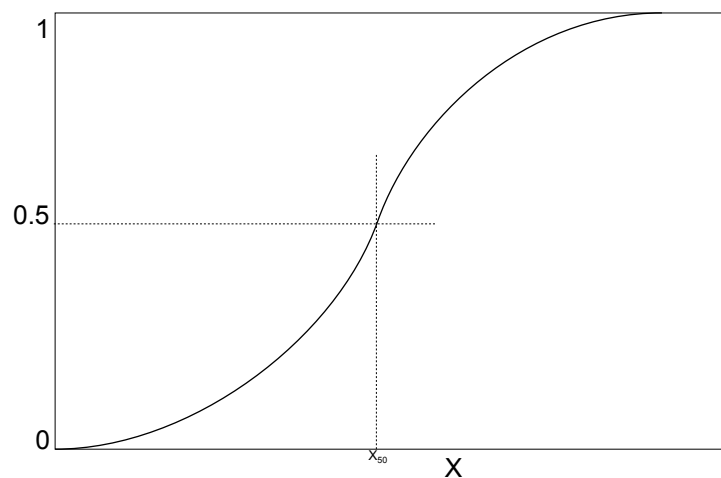
Figure 2.16: A typical grade efficiency curve for a cyclone

2.1.7 Natural length of the vortex

If the cyclone is made longer, this will normally increase the separation efficiency [1], but at a certain length the vortex will attach to the wall, and there is a weaker separation below this point. Figure 1.2 is an example of the "end of the vortex"- phenomenon obtained from CFD experiments. This is a static pressure profile, and one can see that in the middle of the vortex core the pressure is much lower than in the outer areas of the flow. With an occurring end of the vortex, the effect of the cyclone is reduced with more than the shortened length of the cyclone.

The natural length is measured from this point (sometimes called natural turning point) to the tip of the vortex finder (inside the cyclone body). At this position the vortex core rotates with a steady frequency [5] due to the swirling forces. Alexander [6] found that the natural length was a function of the inlet area, the diameter of the cyclone and the diameter of the vortex finder and independent of inlet velocity at a wide range. He found that the length was decreased by large inlets and small outlets.

He introduced the following relationship:

$$\frac{l}{D} = 2.3 \left(\frac{D_x}{D} \right) \left(\frac{D^2}{ab} \right)^{\frac{1}{3}} \tag{2.21}$$

for small cylindrical cyclones.

Bryant et.al (1983)[7] also presented an equation for the natural vortex length:

$$\left(\frac{l}{D} \right) = 2 \left(\frac{A_i}{A_o} \right)^{0.5} \tag{2.22}$$

With A_o being the cross section area and A_i being the inlet cross section area. This equation can also be written:

$$\left(\frac{l}{D} \right) = 2.26 \left(\frac{D_x}{D} \right)^{-1} \left(\frac{D^2}{ab} \right)^{-0.5} \tag{2.23}$$

for easier comparing to the other equations.

Zhongli et.al (1991) [2] made this model for the length:

$$\frac{l}{D} = 2.4 \left(\frac{D_x}{D} \right)^{-2.25} \left(\frac{D^2}{ab} \right)^{-0.361} \tag{2.24}$$

Both equation 2.23 and 2.24 suggest that the vortex length is increased by large inlets and small outlets, which is the exact opposite of what Alexander found in equation 2.21. It is not known why so different results was obtained.

Qian et. al (2005) [8] did a study of the natural vortex length using response surface methodology. They used multiple regression to obtain a second-order response surface model.

$$\begin{aligned}
Y = {} & -3.60 + 2.70x_1 + 0.25x_2 + 3.50x_3 + 0.54x_4 + 1.00x_5 \\
& - 6.45x_1^2 - 0.93x_2^2 - 20.80x_3^2 - 0.03x_4^2 - 0.03x_5^2 \\
& - 0.29x_1x_2 + 4.04x_1x_3 + 0.36x_1x_4 + 0.11x_1x_5 + 0.70x_2x_3 \\
& + 0.49x_2x_4 - 0.08x_2x_5 - 0.047x_3x_4 + 0.73x_3x_5 - 0.06x_4x_5
\end{aligned} \tag{2.25}$$

Where $x_1=D_x/D$, $x_2=a/D$, $x_3=b/D$, $x_4=(h-S)/D$ and $x_5=lnRe$.

As mentioned earlier, the length of the cyclone can not be made arbitrary long. It is possible that other geometrical parameters , and gas velocity, can influence the vortex length, other than the ones given in the previous equations. There has been some other studies considering the cone angle and the efficiency of the cyclone. Xiang et al (2000) studied the efficiency of three cyclones with different diameter for the dust outlet at different flow rates [24]. They found that the collection efficiency was increased when the dust outlet diameter was decreased. This could mean that the cone dimensions are important. CFD simulations of also confirmed this [25].

A study on the effect of inlet dimensions showed that the inlet width was more important than the height, and both tangential velocity and pressure drop was decreased with increasing height and width[26]. The best ratio of width/hight, b/a, was found to be 0.5-0.7.

Numerical simulations of different vortex finder diameters done by Raoufi et al (2007) showed that tangential velocity decreased with increasing vortex finder diameter, which caused lower separation efficiency [27].This was not consistant with the findings of Hoffmann et al (1995) [3].

2.1.8 Roughness

There is always some sort of roughness in a cyclone. Due to erosion and adhesion of particles on the wall (like Hoffmann [3] experienced in his measurements), the surface can also become more rough during operation.

The roughness parameter (k) is defined as the height of one unit of roughness [21]. The friction factor is a function of relative roughness (k/D), where D is the diameter of the pipe) and Reynolds number. A higher friction factor causes the pressure drop in the cyclone to decrease[1], and the the vortex to be less intense.

Kaya et. al (2011) found that the efficiency is influenced by surface roughness [9]. They studied the effect using CFD, and found that surface roughness has a strong effect on the efficiency of the cyclone, and a smaller effect, insignificant on the lowest velocities, on the pressure drop. For higher velocities it was found, as in the theory, that the increase of surface roughness caused a decrease in pressure drop.

Pisarev [10] and Rødland [16] found in their work that the length of the vortex was decreased by increasing surface roughness.

2.2 Computational Fluid Dynamics

CFD has become more and more acknowledged for simulation of flow. The principle is that the area of interest is divided into smaller subdomains and the equations are applied on these and solved for each time step.

In the early days of CFD the user needed to know quite some programming, but now graphic interfaces are available as a commercial software which makes it more user friendly. The software used in this thesis Star Ccm + ver. 06.017 by Cd-Adapco.

2.2.1   Governing equations

CFD is based on the numerical solutions of the Navier-Stokes equations [1]. The equations, written in a finite different form, is then solved for the points of grid covering the area.

The Navier - Stokes equation

$$\rho \frac{D\mathbf{v}}{Dt} = -\boldsymbol{\nabla}p + \mu\boldsymbol{\nabla}^2\mathbf{v} + \rho\mathbf{g} \tag{2.26}$$

The turbulent flow arise as as instability of laminar flow. It is a complex interaction between the inertial and viscous terms of equation 2.26 which is rotational, three dimensional and dependent of time [20].

2.2.2   Turbulence modelling

Turbulent flows can be difficult to model because the flow is highly unsteady, three-dimensional and contains a lot of vorticity [12]. The flow is very complex, it fluctuates over a wide range of length and timescales and can therefor be a challenge to model.

There are different ways to model turbulent flow. In the following some of the most important will be discussed.

Direct Numerical Simulation

In Direct Numerical Simulations, DNS, the Navier-Stokes and continuity equations are solved completely with a three-dimensional and time-dependent solution [20], that means that every motion in the flow is solved and not averaged or approximated [12].

The grid must be fine enough to resolves the smallest scales (kolmogorov length scale) and the domain must be as big as the physical area considered or the largest scales. Because of the high number of cells, this limits the use if DNS to flows with low Reynolds numbers and a simply geometry, because of the number of grid points (and processing speed and computational memory) needed to do the simulation. With DNS one can get very detailed information, if that is needed, but needs to be weighed against the computational cost of the simulation.

Reynolds-Averaged Navier-Stokes

In Reynolds-Avereged Navier-Stokes, RANS, simulations the unsteadiness in turbulence is averaged out [20]. These type of simulations is used for typical engineering purposes, when not all physical quantities is needed. Since the unsteadiness is average out, this can not fully represent the complexity of the turbulent flow. One type of RANS-model is the eddy viscosity model where the effect of turbulence is represented as an increased viscosity [12].

Large-Eddy Simulation

In Large-Eddy Simulation, LES, the large eddies are computed, and the scales smaller than the mesh size are filtered out and modeled with a subgrid-scale model [20]. The larger eddies are computed since they are directly affected by the boundary conditions, while the smallest are less inflicted and only the effect needs to be modeled. This cost

more computational time then the RANS, but is much less costly than DNS. And if the Reynolds number is too high, or the geometry is to complex, this is the preferred option above DNS.

The LES model requires a velocity field with only the components of the large scales. This can be obtained by filtering the Navier-Stokes equations with constant density [12].

Subgrid-scale models

When using LES one would need a subgrid-scale model, SGS, to model the smallest eddies. The first SGS model was made by Smagorinsky in 1963 [20]. It is an eddy viscosity model, which means that the effect of SGS Reynolds stress is mostly from increased transport and dissipation of energy due to the viscosity of the fluid [12]. In this model a parameter, C_s, called the Smagorinsky coefficient, was introduced.

C_s is often set to approximately 0.2 in isotropic turbulence. But C_s is not constant, and may depend on Reynolds number and other non-dimensional parameters. The value also has to be reduced near the wall, and for this the van Driest Damping can be used [12]. This is all implemented with standard values in the commercial software, and can be modified if wanted.

2.2.3 Numerical Solution

After a numerical model is chosen the suitable discretization model needs to be set. The most common ones are finite difference, finite volume and finite element [12]. The software used is this thesis uses the finite volume approach.

The finite difference method is the simplest discretization method, and is best applied on geometries that are not complex. The solution of the the differential equation is approximated at each grid point with the nodal values of the function. Then there is one equation per grid point, and the neighbor nodes are unknown.

In the finite volume method the integral form of the conservation equations are used as the starting point. The domain of interest is divided into smaller domains (control volumes, CV) and the equations are applied to each of those. The value are calculated in the centre of each CV, and interpolations is used to solve the values for the CV surface.

The finite element method is quite similar to the finite volume. The domain is segregated into discrete elements, but the equations are multiplied with a weight function and then integrated over the whole domain.

Meshing

A numerical grid is applied to cover the domain of interest, and is the discrete representation of where the problem is solved [20]. The area is then divided into subdomains at which the equations is solved. The mesh has to be fine enough to get an accurate equation, and as coarse as possible because of the computational effort finer mesh require. Errors due to discretization is reduced when the grid is refined.

The cells can have many types of shape, for instance hexahedra, tetrahedra or blocks [20]. It depends on the geometry which type is best suited. One can also use unstructured grids.

There are different types of meshing models. The models used in this thesis is surface remesher, trimmer and prism layer mesher. The trimmer ensures that the cells does not

Figure 2.17: Mesh applied over the domain of interest, called a volume mesh

exceed the computational domain, and the prism layer mesher makes it possible to have smaller prism shaped cells near the wall.

Time step

To discretizise the equations with time, a time step needs to be set. A normal mistake to do is to set the time step too high, and the solution would not be accurate.

The times step should be set according to the Courant number:

$$\delta t = C \frac{\delta x}{u} \tag{2.27}$$

where δ t is the time step, δ x is the cell size, u is the velocity and C is the Courant number. The Courant should be smaller than 1, and some even say it should be less than 0.5. If the time step is large, the computational effort is smaller, but some of the smaller scales are lost. In the book of Meyers et. al. (2008) [28] the influence of time step on the simulation was investigated. It was stated that when using an implicit time discretization method, time steps that gave a Courant number larger than one could be used. They used courant number of approximately 1, 2 and 5, and found that the was very little difference in the solutions. For the largest Courant number, it showed a convergence behavior that was not as good as for the others. A larger time step required more computational time since the convergence behavior worsened with the size of the Courant number.

Boundary conditions

The boundary conditions of a differential equations are the constraints of the equation, and the solutions need to satisfy these conditions to be valid. In CFD differential equations are solved for each cell, and the cells lying in areas of boundary conditions needs to be treated differently [12], thus different values need to be set at the boundaries.

For a cyclone a velocity inlet and a flow-split outlet (or two, one for overflow and one for underflow) needs to be specified, and the cyclone body set to be walls.

At the inlet quantities as flow direction and velocity needs to be specified, the turbulent intensity also needs to be specified, as well as the turbulent length scale and the velocity. The intensity is given as a percentage, and is normally in the range of 1-10 % in a turbulent flow and the length scale $l = 0.07b$ where b is the inlet width. The velocity can be given as an absolute value, or with specified directions. Normally not much is known about the outlet, and this should be place as far downstream as possible, and the flow directed out of the domain. If there is more than one outlet the split ratio has to be specified. At wall boundary no flow through the wall. A no-slip condition at the wall implies that viscous fluids stick to the wall. Quantities like temperature may also be prescribed at the wall.

Wall laws

If the boundary layer does not need to be resolved, one can apply a wall functions [29] and save computational time.

The turbulent flow is complex, as described in section 2.1.2, there is a close to laminar layer (viscous sublayer) and a buffer layer (log layer)near the wall that needs to be treated differently than the rest of the flow. Depending on the turbulence model, a standard wall law (slope-discontinous between the laminar and turbulent region) or a blended wall law (blends the transition) is used [29].

The basis for the wall functions is the close to linear log region. This can be seen in figure 2.9, the equation is used to "brigde" the wall boundary to the turbulent flow [12].

Convergence

A way of measuring convergence is by doing a grid dependency test. For non-linear problems that are strongly influenced by boundary conditions it can be difficult to show convergence otherwise. A solutions is "converging to a grid-dependent solution" when the solutions is not changing when refining the grid [20]. To check this the same simulations can be run with refined grid for each run, until the solution does not change any more for each refinement.

Another type of convergence is iteration convergence. Most CFD methods require a lot of iterations to converge. The solutions is first guessed and then the iterations systematically improves it [12]. The residual is the difference between the solution of the iteration and the converged solution. This can be watched in a residual plot, when the lines flatten out to a straight line the solution is converged for some models (for example the $k - \epsilon$-model), but different models can have different ways to converge.

For LES the solutions should converge on each time step. A typical residual plot for a converged LES simulation can be seen in figure 2.18. Each top represents one time step [28]. The height of the top is given by the number of iterations per time step (the more iterations the further down the line exceeds).

2.2.4 Errors

Except for the most obvious error, the user error (which should be minimal), there are three types of errors that can occur in a CFD simulation.
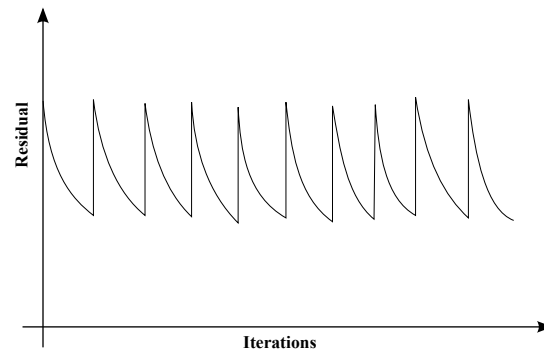
Figure 2.18: The convergence behavior with LES seen in a residual plot. Each peak is one time step, and it converges on each time step.

- The modeling errors is defined as [12]:

   The difference between the real flow and the exact solution of the mathematical model.

   The Navier-Stokes equations is considered exact, but for most engineering purposes these are not fully solved. The laws of Newton and Fourier are, as the simulations that are made, models. Even though they are based on experimental observations, all the properties of the fluid may not be known [12]. There can be difficulty defining the initial and boundary conditions, and for this reason the simulation may have modeling errors.

   The geometry can also be a challenge to fully represent in the model.

- The discretization error is defined as [12]:

   The difference between the exact solution of the governing equations and the exact solution of the discrete approximation.

   Which means that there is an error associated with the choice of discretization method. All numerical methods have a approximated solution. Using better approximations can increase the accuracy, thus it needs more computation time and are more difficult to program. Both the cell size and time step can inflict this.

- The iteration error is defined as [12]:

   The difference between the exact and the iterative solutions of the discretized equations.

   After the discretization, some non-linear algebraic equations has to be lineararized and solved. Solving these requires a number of iterations, but this can't be infinite, and a convergence criterion can be set to decide when to stop the process.

All numerical solutions will contain errors, but is important to try to keep them at an acceptable level.

Chapter 3

Literature Survey

The following chapter will give a presentation of studies of the vortex length in a cyclone separator, but also CFD modeling of cyclones in general.

3.1 End of the vortex phenomenon and the natural vortex length

Previous research has been done on finding a model for the length of the vortex. Since the natural vortex length is related to efficiency, studies concerning cyclone efficiency are also relevant.

3.1.1 Alexander et. al.

Alexander [6] was one of the researchers laying the ground work of cyclone theory. He did experimens on fairly small, cylindrical cyclones with diameters in the range approximately 30-50 mm in diameter. His equation(2.21) will therefore not be valid for all operating cyclones today. But he did important research about flow in cyclones, not only about the vortex length, which gives a better understanding and was used as a basis for many studies after him.

He found that it is likely that a small vortex finder diameter gives a high separation efficiency. Through experiments it was found that high efficiency was given by small inlets, but a requirement of a certain flow rate set a boundary of how small it could be. It was assumed that the inlet area is three quarters of the vortex finder diameter, square and helical, was the most effective.

He defines the natural vortex length as the distance from the bottom of the vortex finder to the point where the vortex turns. It is also stated that measurements are not easily acquired since the vortex end deviates up and down over range of approximately one quarter of the cyclone diameter.

It was observed that large inlet and small outlet cause a shortening of the natural vortex length.

3.1.2 Bryant et. al.

Bryant et. al. [7] carried out experiments and visually determined the length of the vortex. They fitted an expression for the empirically obtained results., and also performed

experiments to show that the position of the end of the vortex is independent of inlet velocity under normal operation conditions. The differences between the theoretical length (as calculated from Alexanders equation) and the length measured from erosion in the cone and particles attached to the wall. It was observed that a reduction of vortex finder diameter caused a longer natural length (which is the exact opposite of what was observed by Alexander). The cyclones that was used had a long cylindrical area, and was closer to a swirl tube (but with a tangential inlet), than a cylinder on cone.

3.1.3 Zhongli et. al.

Zhongli et. al. [2] did experiments on long plexiglass cyclones. They proposed an equation suggesting the natural vortex length was longer than Alexanders.

Experiments were completed with both cylindrical and conical cyclone models. The tangential velocity and static pressure was measured with a five-hole pitot probe, and the tangential velocity was seen to decline with axial direction. By applying dust to the cyclone, the vortex was visualized, and a stable dust ring was seen indicating the natural turning point. It was found that the natural length was slightly lengthened by the increase of inlet velocity. Larger inlet areas also prolonged the vortex length.

They also observed that a conical cyclone also had a longer natural length than a cylindrical one with the same dimensions except the dust outlet diameter.

An experimental performance study was also conducted with a very low particle concentration [30]. In this study they found that the collection efficiency increased with particle concentration, and the efficiencies for different inlet velocities became closer to each other (as opposed to better separation efficiency with higher inlet velocities).

3.1.4 Hoffmann et. al.

Hoffmann et. al [3] did experiments using glass cyclones, and smoke to visualize the vortex. They used a geometry called the Stairmand HE, with a diameter of 0.2 m. Different vortex finder diameters and different lengths of the vortex finder was tested to see the influence on the vortex length. A tube section was placed beneath the conical section for preventing the collected dust from being re-captured in the vortex. The stable vortex position was often found in the tube section. Smoke was injected to visualize the flow pattern. It was said to disturb the flow initially, but the position to where the smoke extended was seen fairly clair after a steady-state for pattern was established. The smoke left a paraffin containing layer, at which the flow pattern at the wall could be seen. With higher inlet velocity a ring formed at a stable position indicating the length of the vortex. However, the ring seemed to appear a few centimeters above the smoke shaft. It was observed that the ring moved lower as the coating dried, which was set in relation to the apparent roughness that arose because of the layer. Therefor it was shown that the vortex end was dependent of roughness. The natural length was seen to be longer with larger vortex finder diameter, and inlet velocities. Alexanders equation also suggest that the natural length is longer with larger diameters, but predicted a shorter vortex than measured in the experiments. There was not found any consistent relation between the length of the vortex finder and the natural length, and it was suggested that the length should be measured from the roof if the cyclone and not the tip of the vortex finder. By using dust instead of smoke, the same phenomena was observed; An amount of dust was

attached to the wall at at certain position. With a heavy dust loading, the position of the vortex was further up in the cyclone than without the dust.

Some experiments was also done in very long cyclones (approximately 1.5 m). It was seen that the end of the vortex position was independent of inlet velocity, but only in the longest cyclones. It was also suggested that since a conical section stabilized the vortex, the configuration should also be taken into account.

3.1.5 Peng et. al.

Peng et. al. [5] used a stroboscope to visualize the vortex in cylinder-on-cone cyclones and swirl tubes, and pressure transducers to measure pressure in the cyclone. When using the stroboscope a ring could be seen in dust on the wall, which was the core of the vortex ("eye of the hurricane"). They used pressure transducers to detect the rotation frequency of the vortex core. In the middle of the core there is low pressure and the rotations could be measured as a sudden drop in pressure each time the vortex passed. By using multiple transducer placed vertically along the cyclone body a pressure profile for the vortex was obtained.

3.1.6 Qian et. al.

Qian et. al [8] used response surface design on their experiments to obtain a new model for the vortex length using CFD simulations. A Reynolds stress transport (RSM) model was used. The variables chosen to vary was vortex finder diameter (D_x), inlet length (a), inlet width (b), cylindrical section beneath the vortex finder ($h - S$) and Reynolds number (Re). They found that the natural length slightly varies with the inlet velocity, and that with increasing vortex finder diameter the length is increased to a certain point and after this it becomes shorter. For the inlet area the findings was consistent with the ones of Alexander, smaller inlet areas results in a increase of the length. The experiments was performed on purely cylindrical cyclones. And also in all the experiments the vortex ended in the tube under the cyclone body.

An experimental study concerning effects of the inlet section angle on the separation performance was also performed [31]. Normally the inlet section is perpendicular to the cyclone body, but in this study other angles was tested. They found that the tangential velocity decreased in some regions with increasing angle. The tangential velocity increased in the downward flow; the outer vortex increased and the inner vortex decreased in tangential velocity. They also found that the pressure drop was reduced compared to an normal cyclone, and this difference increased with larger angels, and the separation efficiency also had a great increase. Using CFD and a response surface methodology the inlet section angle could be studied more comprehensively [32], they found that the the conventional cyclone had a stronger short cut flow rate than the cyclones with angled inlets. The vortex length was not studied in this case.

3.1.7 Previous work done in cyclone group at the University of Bergen

Vidar Gjerde [15] did a study of the end of the vortex in his master thesis. He did measurements of different lengths up to 165 cm of swirl tubes by connecting different sizes of shorter tubes. He found that for a range of tube lengths the vortex core would

centralize if the flow rate was high enough, and this was close to linearly dependent on the tube length. Since the connections between the tubes seemed to have an interference with the flow rate needed for centralization (the more connections the higher the flow rate, also for the same total tube length), it was needed to do new experiments without the connections. A comparison with newer results is done in chapter 7.

Experimental measurements on the end of the vortex in this thesis was done in collaboration with Torill Rødland, see chapter 4. Rødland and Gleb Pisarev continued the experimental work on swirl tubes by investigating the effect of surface roughness on the end of the vortex in swirl tubes. Most of the work is described in Rødlands master thesis [16]. They used the same swirl tubes as used earlier, only with a certain wall roughness. The roughness was made by coating the tube with metal particles of known size, or by using sand paper on the inside of the tube. Measurements was then taken to see at which flow rate the vortex centralized compared to the tubes with smooth walls. They did measurements on tubes of 60 and 80 cm length.

For the walls treated with sandpaper, and a surface roughness of approximately 0.1 - 0.2 mm, the flow rate needed for centralization was the same as for smooth walls, only an increase of time was found. The coated walls had a mean roughness height of 0.18 - 0.2 mm. With this roughness a clear distinction was found from smooth walls. A much higher flow rate was needed for the vortex to centralize, and for the 80 cm tube they tested even higher flow rates and the the vortex did not centralize in any of the experiments.

CFD simulations was also performed. By changing the wall function coefficient, E, a surface roughness was obtained in the simulation. It was done simulations for smooth walls, and walls with a roughness of 0.1 mm and 0.2 mm, with different inlet velocities. They gave the same result as in the experiments. Pisarev et. al. [10] did simulations on 80 cm tubes, and the same trend was seen.

Pisarev also did a study of the length of the vortex in swirl tubes in the PhD thesis [33]. He found that if the vortex was not centralized, but attached at a stable position at the wall, the position where is attached was independent of flow rate and cyclone length.

3.2 Computational fluid dynamics on cyclones

3.2.1 Griffiths et. al.

Griffiths et. al. performed a study using CFD to model cyclone performance in small sampling cyclones [34]. They mention that the $k - \epsilon$ model causes excessive levels of turbulent viscosity and an unrealistic tangential velocity distribution [35] and can therefor not be used. Since the Reynolds Stress models at the time was very computational expensive, a RNG-based $k - \epsilon$-model was used; a mathematically simple (like the $k - \epsilon$) and accurate (like the Reynold Stress) model. They found that the CFD model predicted pressure drops, and the flow field in great detail. With this the performance of the cyclones could be investigated.

3.2.2 Hoekstra et. al.

Hoekstra et. al. did an experimental study which was verified with CFD simulations [36]. He used cyclones of 0.29 m in diameter with a scroll type of inlet. The cyclones had a

long cylindrical section, completed with a short conical section. Experiments was carried out with a Reynolds number of 2.5×10^4. Tangential and axial velocity components along the radius was measured using laser-Doppler velocimetry (LDV). CFD simulations was then carried out using different turbulence models. The different turbulence models used where $k - \epsilon$-model, RNG-$k - \epsilon$-model, and Reynolds Stress Transport Model (RSTM). By comparing the experiment with the CFD simulations carried out with RSTM, he found that they where in reasonable agreement. The other turbulence models did not show a realistic presentation of the axial and tangential velocity, and was therefor not suitable for turbulent flow.

In his PhD thesis [37] Hoekstra did an extensive study on cyclone efficiency both experimental and by using CFD. The gas flow field was studied experimentally using Laser-Doppler Anemometry (LDA) and he found a low-frequency instability, related to a phenomena called the precessing vortex core (PVC). This PVC-phenomena was furthers studied using laser visualization.

Different CFD simulations was run to using different models compare with the experimental data, a good agreement was found when using a Reynolds Stress transport model, and the LES-model was found to also being able to model the precessing motion of the vortex core. From this a regression model was made to describe the collection efficiency of the cyclone. A response surface model (to test different geometric variables and operating conditions) was also made from which one could calculate the pressure drop and cut-size of the Stairmand cyclone.

3.2.3   Derksen et. al.

Derksen et. al used LES [38] to simulate turbulent flow in a reversed-flow cyclone. The cyclone was of the swirl tube type, but with a tangential (scroll-type) inlet, and the Re of the flow was 1.4×10^4. A three diminutional simulation with high resolutions was used, and it was found that a axis-symetric model would not properly model the swirling flow. Good agreement with LDV-experiments executed by Hoekstra [36] was found.The study also included simulations with particles in the flow, and it was found that particles larger 10 μ m did not need any special modeling. But smaller particles would influence the sub grid-scale of LES and this had to be taken in to account. It was mentioned that higher (and more common in industrial cyclones) Re number, was not straight-forward using a uniformly spaced grid because of the resolution in the boundary layer. Locally refined grid was recommended as a solution.

A more extensive study simulations using LES was then done [39]. It is mentioned that using LES on swirling flow is better than using RANS - models because flow containg particles is more realistically modeled with LES, also swirling flow often experience coherent, quasi-periodic fluctuations (like precceing vortex core, PVC) which LES simulates better than RANS. Three different SGS-models where used, with the same damping function. For supplementary information about turbulence modeling see section 2.2.2. Different simulations where carried out using various SGS-models, Re number, grid spacing, vortex finder diameter and inlet velocity. They also observed the phenomena vortex breakdown in the simulations. When the size of the vortex finder diameter was tested, they found that the axial velocity was strongly dependent of this and also the axial position of the vortex tube. The Mixed-Scale-model (MSM) was the best SGS-model tested.

They also did a comparison of different modeling approaches for turbulent flow, and found that LES revealed more of the physics in turbulent flow than other models, but at a computational cost [40][41].

Chapter 4

Experimental setup

The experimental work was done in collaboration with Torill Rødland and Gleb Pisarev. The rig was built at the University of Bergen during previous projects.

The pump had an effect of 7.5 kW and the air moved through the system by suction. Rough adjustments of the flow rate was done by using the main flow valve, and fine-tuning with the bypass valve, see figure 4.1 for draft of the entire set up.
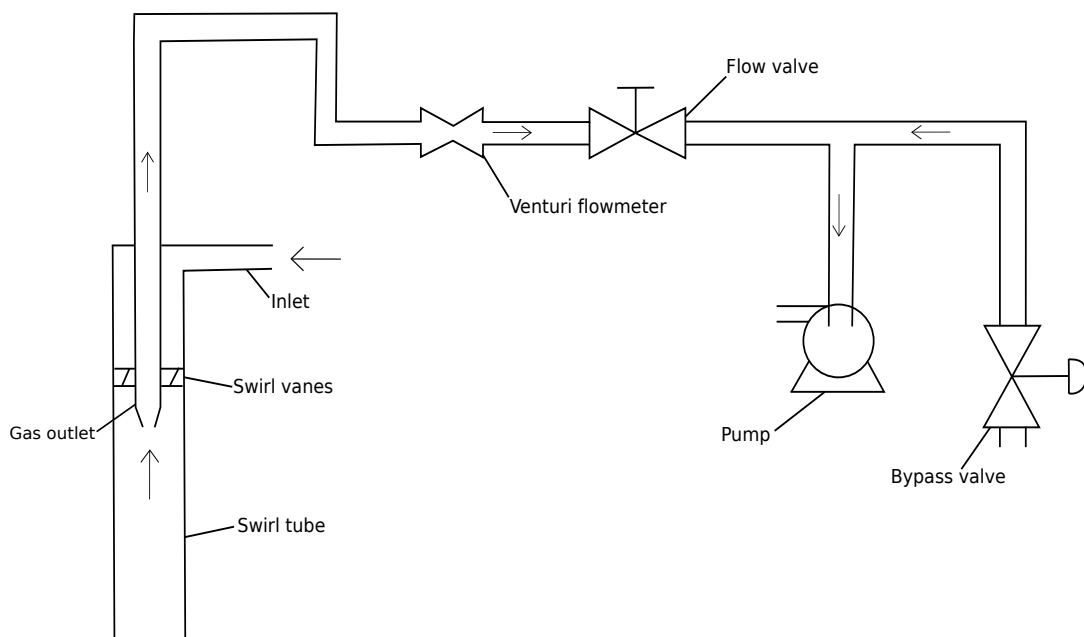
Figure 4.1: Swirl tube set up used in experiments

The swirl tube body, made of plexi glass, was interchangeable so different lengths could be tested, but all with the same diameter of 10 cm. The vortex finder diameter is 6.5 cm, but a narrows in at the tip. Swirl vanes surrounding the vortex finder have a length of 6 cm and a width of 1.25 cm and are 1.75 cm apart. The tubes has an estimated roughness of 1 μm. There was no dust hopper in the experimental rig, this is because the separation efficiency was not to be measured and for the least interference with the flow pattern. A venturi flow meter measures the gas flow rate, and pressure taps situated vertically along the swirl tube body measured the pressure at specific positions.

4.0.4 Flow rate measurements

Measurements of different flow rate was done to find the centralization flow rate at each tube length. They flow rate was measured using a venturi flow meter. There are two tubes in the venturi flow meter, one connected ahead of the the venturi, and one at the throat of the meter. The pressure difference between these two is measured as a voltage. There is a certain voltage when there is no flow (U_0). This value has to be subtracted from the measured value with flow. 1 V corresponds to 43.75 mbar (4375 Pa).

The pressure difference in pascal in the venturi meter is given as:

$$\Delta p = (U_{measured} - U_0) \cdot 4375 \tag{4.1}$$

Since the flow rate is the same in position 1 and 2, and by using Bernoullis equation (equation 2.15), the flow rate is given as:

$$Q = V_1 A_1 = V_2 A_2 = A_2 \sqrt{\frac{2 \left(p_1 - p_2\right)}{\rho \left(1 - \left(\frac{A_2}{A_1}\right)^2\right)} \cdot 3600} \tag{4.2}$$

where $(p_1 - p_2) = \Delta p$, A is the cross section area and V is the velocity. Venturi meters often have a discharge coefficient, c_d which has to be multiplied with the flow rate. c_d for the venturi meter used in this experiment is 0.90.

Cyclone tube length of approximately the same length as used in Gjerde's master thesis [15], was used and the results can be compared and one could see the influence of having connections in the tube. By adding small particles (sand), the vortex could be visualized.

4.0.5 Measurements with pressure transducers

Pressure taps vertically attached to the swirl tube body made it possible to measure the pressure drop as the vortex core move passed the measuring point. One could then see where the vortex core first bent to the wall, and by comparing different results; if this was independent of inlet velocity.

The pressure taps where axial placed 3 cm apart on the cyclone body, and one position at a time could be measured. The program LabView was used to log the data, and each measurement lasted approximately 10 seconds with 1-2 seconds before starting the pump connected to the system. When the vortex core passes the pressure taps, this can be seen as a pressure drop in the measurements. The frequency at which the vortex core rotates can also be seen. Two measurements are shown in the output windows in LabView, a pressure measurement of the inlet flow and one of the selected pressure tap on the cyclone body. Since the length of the vortex is given from the vortex finder (same position as the swirl vanes), the position the the pressure tap are given as a position below the swirl vanes.

If a pressure tap over the natural turning point was selected, a pressure drop was registered as the vortex core passed down. Then a new measurement was done with the same flow rate, but with a pressure tap further down. This was continued until a stable position (if excisted) was found.

Chapter 5

Development of computational techniques and design of numerical experiments

Methods for design of experiments is given in this chapter together with an introduction to near wall meshing and modeling roughness in CFD.

5.1   Design of experiments

When planning a set of experiments (a design of experiments), there is different factors (variables) that is desirable to change over a number of levels. Examples of factors can be quantitative variables like different temperature or concentration, or qualitative variables like presence or absence of catalyst [42]. By changing one factor at a time while holding the others constant, not all information is obtained about the factors [43]. It is therefor important to do a proper planning and design of the experiments. It is called a factorial scheme when all the variables are tested with each other at all levels. An advantage of using a factorial scheme is that the interactions between the factors can be measured [42].

In this thesis a factorial scheme is used on the CFD simulations, because of this the experimental error (other than numerical present in the simulations) and reproducibility of the experiment does not need to be taken into account.

5.1.1   Factorial design

A full factorial design is to run a set of experiments with all possible combinations of factors and levels [42]. Each run is called a treatment [44], which is a specific combination of levels for each factor. For a complete factorial design, one would need as many treatments as there are combinations of levels and factors.

The number of experiments required to have a full factorial design is found in equation 5.1.

$$Experiments = levels^{factors} \tag{5.1}$$

That means if there is 7 factors to investigate at two levels this would require $2^7{=}128$ number of experiments. But there can be reductions to this (see next section). When doing a set of experiments, one wants to find out which of the factors that cause the main effects for the result, and if there is any interactions between the factors. Main

effects are the factors that are significantly important to the results, but there can also be interactions between the factors that can be significant [45].

5.1.2 Fractional factorial design

A fractional factorial can be used when there is a large number of variables, this can help screen for which are the significant ones [42]. And it is not alway necessary to know for example all the two or three factor interactions.

Two level fractional design for up to 7 factors with 8 runs can be constructed from table 5.1. One does not need to use the whole table. For less than 7 variables, the n-1 first columns and the last one are used. To set up a two level factorial design of experiments with up to seven different variables in only eight runs, table 5.1 can be used. Only the first 3 three main effects does not overlap with a two factor interction. The first there columns are used first, if a fourth is needed the last one is used, and after this column number four, five and six is used.

This can be used for screening purposes two find which variables are significant and need further investigation.

Table 5.1: Two level factorial design of eight runs with up to 7 variables [42]

Run no.	a	b	c	ab	ac	bc	abc
1	-	-	-	+	+	+	-
2	+	-	-	-	-	+	+
3	-	+	-	-	+	-	+
4	+	+	-	+	-	-	-
5	-	-	+	+	-	-	+
6	+	-	+	-	+	-	-
7	-	+	+	-	-	+	-
8	+	+	+	+	+	+	+

For mixed level design a more advanced scheme has to be made. Because of the large number of experiments required, response surface designs are often recommend [43].

5.1.3 Response Surface Methodology

When planning a set of experiments, different factors can effect the outcome: Other variables should have been considered, for example different ranges of the levels or other models should have been considered. But if an iterative scheme is used, with sequences of experiments, the experiments will more surely head in the same direction even from a different starting point [42]. This is why response surface methods sometimes should be used on set of experiments that are complex and have a many variables. The difference from a factorial scheme is that a linear correlation is not assumed, and the response is on a surface and not necessarily a plane. With a factorial design, there is no way to

know if the optimum is local without doing more experiments to see if the range should be different.

If a process yield is a function of different levels of two variables

$$y = f(x_1, x_2) + \epsilon \tag{5.2}$$

where ϵ is the observed noise or error on the response y [43]. Then the response surface (the expected response) is

$$\eta = f(x_1, x_2) \tag{5.3}$$

The response surface can be fitted by a polynomial.

A first order model is normally fitted first, but if the surface has a curvature, higher order models need to be used [46].

A second order model is given by:

$$y = \beta_0 + \sum_{i=1}^{k} \beta_i x_i + \sum_{i=1}^{k} \beta_{ii} x_i^2 + \sum_{i=1}^{k-1} \sum_{j=2, i<j}^{k} \beta_{ij} x_i x_j + \varepsilon \tag{5.4}$$

where x_1, x_2, ..., x_k are the variables (factors) that influence the response y, β_0, β_i (i = 1, 2, ..., k), β_{ij} (i = 1, 2, ..., k; j = 1, 2, ..., k) are unknown parameters and ε is the error.

In a second order design, the number of points in the design must be at least

$$p = (k+1)(k+2)/2 \tag{5.5}$$

where k is the number of variables.

Central composit design

An alternative to doing a reduced (or full) factorial design is the central composite design [47]. When dealing with three or more levels, the number of runs will be very high for a factorial design, and therefor a central composite design is more convenient because of the smaller number of runs.

This design consist of:

1. A 2^k full factorial design with the coded values -1, +1. This is forming the "cube" (at least for k = 3), and is the factorial portion of the design.

2. n_0 center point(s) at (0,0, ...,0)

3. $2k$ axial points at the coordinates ($\pm\alpha$,0, ...,0), (0, $\pm\alpha$, ...,0), ..., (0,0,..., $\pm\alpha$). This is the "star" or axial portion of the design.

This makes the total number of runs $N = 2^k + 2k + n_0$ [46], which is a small number compared to a full factorial design for designs with many variables. Multiple number of center points is normally used if the experiments are not run at the same time (within a reasonable amount of time), and one center point for each batch of experiments can be used. This is not applicable when the experiments are CFD, which have no environmental influence. If the the values in the experiments can not exceed the given range, then $\alpha =$

1. This is called a face center cube, where the axial point is at the center of the faces, and not outside the cube [48]. For theory about other values of α, see the books of Box and Draper (1987) [47] or Khuri et. al. (1987) [46].

For a three dimensional case (three variables). The central composite design can be seen as a cube, with the center points forming a cross inside the cube, as seen in figure 5.1
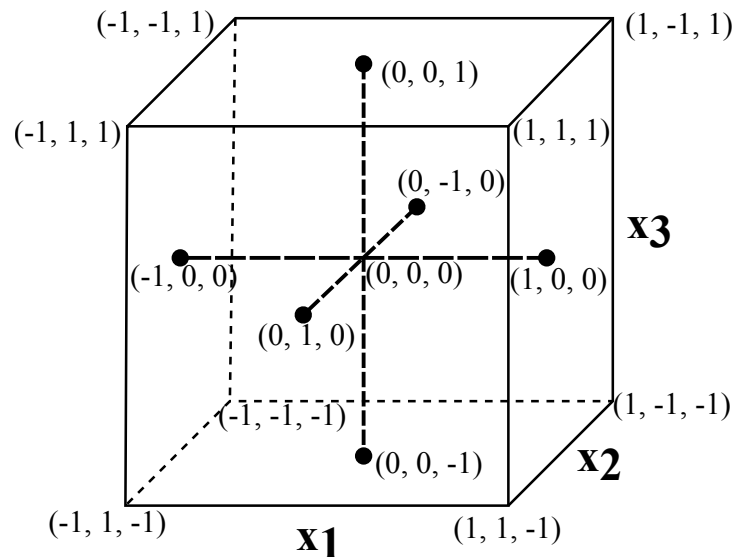
Figure 5.1: A schematic of a central composite design of three variables with high and low value, a center point and axial points [47], [46].

5.2 Near wall meshing

Local refinement can be done on important parts of the geometry, instead of refining the whole area, to get the total number of cells as low as possible. It is important to use prism layers near the wall to accurately model the turbulent flow. A prism layer is orthogonal prismatic cells close to the wall, where a different size than the core cells can be used [29]. Because of the nature of turbulence, special approach is use for near wall modeling. There are two different approaches for near wall meshing, two-layer model or a wall function model [49].

If the boundary layer needs to be resolved (wall $y+ \approx 1$) the first grid point near the wall must to be very small (often in the order of 10^{-5}m),in order to resolve the smallest eddies. By using prism layers near wall layers are refined, keeping the bulk cells bigger. Only the near wall cells needs to be this small. The cells are made gradually larger closer to the turbulent core, covering the boundary layer area. The first layer thickness is set accordingly to the wanted $y+$ value (use equation 5.6), the number of prism layers are chosen and the total thickness of the layers. It is normal to use 10-25 prism layers that covers the boundary layer. In theory this approach is sometimes reffered to as a two-layer zonal approach, where the first "layer" is the 10-25 prism layers covering the boundary area.

For cases where the boundary layers does not need to be resolved, wall functions are used, see section 2.2.3. For a turbulence model using wall functions, a normal number of

prism layer is 1-3 [29]. For most cases, one does not need to resolve the boundary layer, the wall function model can be used and the wall $y+$ value can lie within 30-100 [49], saving a lot of computational time.

The wall distance needed for a specific $y+$ value at the wall is given in equation 2.10. Rearrange the equation and solve for y, which is the wall distance, and where the first grid point must be placed to achieve the specific $y+$ value. This value is in the center of the cell, and the prism layers thickness is set to twice this size.

$$y = \frac{y^+ \mu}{\rho u_*} \tag{5.6}$$

The wall shear stress, τ_w, can be found from equation 5.7

$$\tau_w = C_f \frac{1}{2} \rho v^2 \tag{5.7}$$

where C_f is the skin friction that can be found from for instance the Schlichting skin-friction correlation for $Re < 10^9$

$$C_f = [2log_{10}(Re_x) - 0.65]^{-2.3} \tag{5.8}$$

Re can be found from equation 2.1, with the boundary layer length as D, and free stream velocity as v. For a cyclone the diameter of the cyclone body is most suitable to use as the boundary layer length.

One reason to resolve the boundary layer is for instance to look at the heat flux across the boundary layer.

5.3   Modelling roughness

The velocity distribution is modeled as:

$$u^+ = \frac{1}{k} ln\left(E' y^+\right) \tag{5.9}$$

where u^+ and y^+ is given in equation 2.9 and 2.10, and E' is the modified log-law coefficient given as

$$E' = \frac{E}{f} \tag{5.10}$$

In Star Ccm+ the default values of k = 0.42 and E = 0.9 [29]. f is a function of the roughness parameter:

$$R^+ = \frac{r u^*}{\nu} \tag{5.11}$$

where r is the equivalent sand-grain roughness, u* is given in equation 2.8 and ν is the kinematic viscosity. f is unity for smooth walls, and for rough walls it is computed according to:

$$f = \begin{cases} \left[B\left(\frac{R^+ - R^+_{smooth}}{R^+_{rough} - R^+_{smooth}}\right) + CR^+\right]^a & for R^+_{smooth} < R^+ < R^+_{rough} \\ B + CR^+ & for R^+ > R^+_{rough} \end{cases} \tag{5.12}$$

where a is

$$a = sin \left(\frac{\pi}{2} \frac{log \left[R^+/R^+_{smooth} \right]}{log \left[R^+_{rough}/R^+_{smooth} \right]} \right) \tag{5.13}$$

The default values in Star Ccm+ is: B = 0, $R^+_{smooth} = 2.25$, $R^+_{rough} = 90$ [29].

In RANS models the roughness can be set directly in the program. For the other models the roughness can implemented by changing the wall function coefficient, E.

Chapter 6

Computational Simulations

In order to study the confined swirling flow in a cyclone, a CFD model has to be carefully built. One of the most important decisions is the turbulence model. A correct turbulence model has to be used, and a numerical grid has to be placed over the domain of interest. LES was chosen as a turbulence model, because of the good agreement it has shown. It also has to be decided how the near wall interaction wants to be handled, and if the boundary layer should be resolved or not.

6.1   Setup

A lot of different parameters has to be set in the software for the computational calculations are executed in a manner that will best represent the real flow and its nature.The mesh models for the numerical grid that was used was the remeshed surface, trimmer and prism layer. This ensured that the computational grid did not exceed the domain, and one could make a refinement of the cells near the wall.

The physics models used where three dimensional, constant density, all y+ wall treatment, Large Eddy simulations and Smagorinsky subgrid scale. A segregated solver was chosen, which calculated the pressure and velocity components uncoupled, and 5 iterations per time step was used. The all $y+$ wall treatment made it possible to not model the boundary layers near the wall, but start at a higher $y+$ value (larger cells near the wall). Under-relaxation factors of 0.5 for the velocity and 0.2 for the pressure was also used to stabilize the solution. A no-slip condition was prescribed at the walls, which is a shear stress specification. In a no-slip wall, the tangential velocity of the fluid is set to zero at the wall, and the viscosity is important here [29]. An initial pressure of 1 bar was set, which is a normal operating pressure. It was tried to apply a coarser grid on the lower part of the cyclone (cylindrical section under the cyclone body and dust hopper), to have a smaller total number of cells, but this was not successful. The flow pattern changed in the cyclone, probably due to the poor modeling in the lower part.

6.2   Simulations

The time step was set using the equation 2.27, and an appropriate time step was found for Courant number = 1.5. The Courant number is a function of cell size, and an appropriate cell size for the core cells (that had an y+ value higher than 70) was used

to get the wanted Courant number and a large as possible time step.).

A test to see if the resolution of the boundary layer has any influence of the natural length was performed. Two simulations was made one using the wall function (wall y+ value ≈ 30) and one where the boundary layer was resolved (wall y+ ≈ 1, two-layer model). For the test simulations an inlet velocity of 10 m/s was applied. The grid size for the near wall layer was found by calculating the necessary wall distance to the first node by using equation 5.6. The first node distance was 0.055 mm from the boundary layer model with 10 prism layers of a total thickness of 3.5 mm (y+ ≈ 65, covers the boundary layer area). For the model using wall functions the near wall thickness was 1.8 mm with only 2 prism layers of a total thickness of 4.25 mm. This is shown in figure 6.1.

(a) Mesh for resolving boundary layer   (b) Mesh for using wall functions
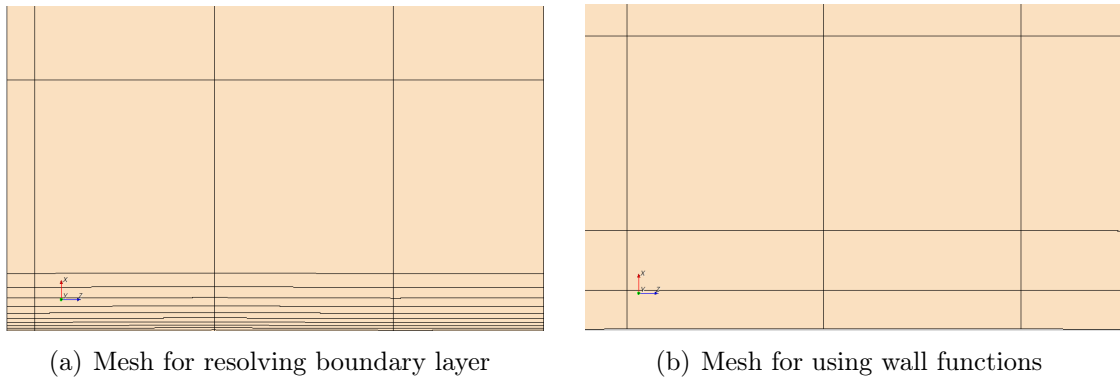
Figure 6.1: Mesh profiles for resolved and unresolved boundary layer

By setting the size of the prism layer thickness to an absolute value and not a percentage of the cell base size, a grid dependency test could be performed without changing the wall y+ values. Both simulations where run with 4.5 mm cells, which corresponds to a y+ value of 75 which is in the turbulent core, and therefor applicable to use. Both simulations gave the same length of the vortex, and the wall function model was applied to all simulations.

Four simulations with varying total thickness and number of prism layers was tested to see the influence on the cortex length. The thickness and number of prism layers can be seen in table 6.1. The near wall thickness was set to 3.5×10^{-5}m for all the experiments with prism layers.

Table 6.1: Prism layer test

Experiment	Prism layers	Total layer thickness
a	0	-
b	2	0.1 mm
c	3	0.5 mm
d	5	1 mm

Since the Courant number changes with the velocity, the cell size had to be adjusted accordingly when the velocity was changed.

6.2.1 The Hoffmann cyclone
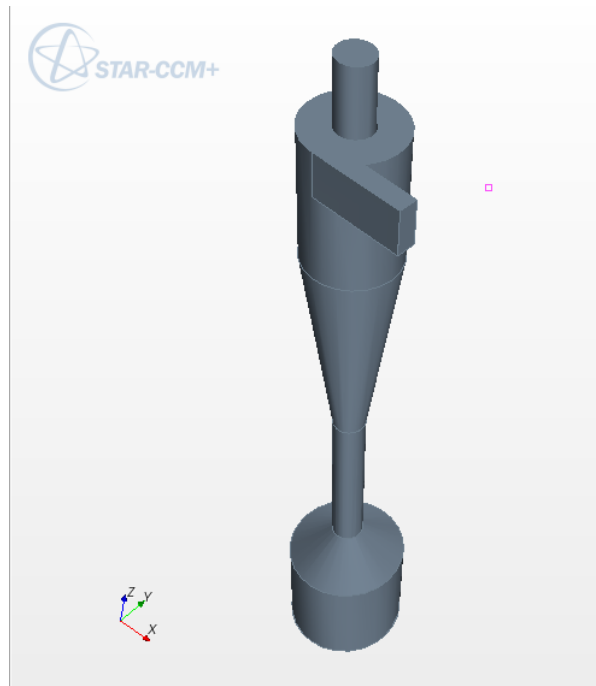
Figure 6.2: Geometry of a Hoffmann cyclone, built in Star Ccm+.

The geometry was built in the 3D cad part in Star Ccm +. The first geometry that was built had the same dimensions as in Hoffmann (1995) [3] for comparison with experimental results and can be seen in figure 6.2. In this thesis the cyclone with these dimensions will be referred to as the Hoffmann cyclone.

The diameter of the cyclones are 0.2 m, the vortex finder diameters for the two cyclones simulated are 0.075, all the other dimensions are of the Stairmand HE design. The vortex finder length was respectively 0.25.

In the experiments [3] the vortex ended almost every time in the cylindrical section. Since the simulations are done with only a gas flow, and not smoke of vaporized paraffin (with higher density), the vortex length is excepted to be shorter than in the experiments.

The grid dependency test showed that by comparing the velocity profile a suitable cell size where to solutions does not change is 4.5 mm. The total number of cells for each cell size can be seen in table 6.2. Wall functions where used (all y+ wall treatment), and first node was set as described in previous section. The simulated gas inlet velocities where 5, 10, 15, 20, 25 and 30 m/s. With each of the inlet velocities, a new wall $y+$ value, and courant number, was calculated. The cell size and time step was adjusted according to this.

Table 6.2: Grid dependency test

Cell size	6 mm	5 mm	4.5 mm	4 mm	3.5 mm
Number of cells	230 000	375 000	498 000	690 000	990 000

6.2.2 New model for the natural length

In order to find a new model for the natural vortex length, factorial design scheme was set up. A central composite design, for experiments to test the whole range of different geometries and inlet velocities was used. 5 variables was chosen, and the rest of the design variables was set constant according to a Stairmand HE cyclone (see table 2.1. Since the length of the vortex is measured from the tip of the vortex finder, S can be held constant. The variables where made dimensionless by dividing them with D, but the diameter for all cyclones is set to 0.2 (for easier comparison with the Hoffmann cyclone). See table 6.3 for the constant dimensions and parameters. The turbulent length scale was set to 0.07b.

Table 6.3: Constant dimensions and parameters

D	0.2 m
S	0.1 m
D_d	0.07 m
ρ	1.18
i	0.04

The Reynolds number was varied by changing the dynamic viscosity, μ, from high value of $Re = 3 \times 10^6$ to low value of $Re = 3 \times 10^4$ with inlet gas velocities of respectively 25 and 5 m/s. For the center points the middle value was used.

The different variables of the cyclone geometry can be seen in table 2.1. It was desirable to vary the design of the testing cyclones with the range of the design in this table, but since the largest inlets did not fit on the cyclones with the smallest value of $H - H_c$ (exceeded to the conical part) it was decided to not take in to account the inlets positioned outside the cyclone body (Tengbergen B, Stairmand HF and Vibco). Also the the smallest value for $H - H_c/D$ was increased from 0.25 to 0.7, which is the second smallest in table 2.1. This is done because the cyclones then fit a larger inlet area. The range of vortex finder diameter was also reduced for the same reason, but still the design would cover a great range of operational cyclone geometries. WIth a large inlet area the flow would inflict with the large vortex finder, and therefor the sum of the largest inlet width and vortex finder radius is one cyclone body radius. The largest value for inlet area that fits on the lowest value of $H - H_c/D$ and highest value of D_x/D is used as high value for the inlet area.

It was wanted to cover a larger range of the geometrical parameters and Reynolds number, but this resulted in some of the cyclones did not form a vortex. When using the smallest inlet, the largest cylindrical section and the smallest Re, the vortex did not form. Therefor approximately the same range as Hoekstra used in his thesis[37] was also used in this thesis, since this has already been proven to work.

In the previous equations for the natural length only inlet area, vortex finder diameter and body diameter is taken into account. In this experiment we want to see if any other variables is significant for the length of the vortex. Pisarev et al. (2010) found that in cylindrical cyclones the position of the vortex end was independent of flow rate (inlet

velocity)[14]. But this is not consistent with findings in this thesis concerning cylinder-on-cone cyclones. Qian et. al. [8] performed CFD simulations with cylindrical cyclones and found the length to be dependent of inlet velocity.

A full factorial design of 5 variables with 3 levels would be $3^5 = 243$ experiments, which would cost too much resources and time. A central composite design would therefor be more applicable. A central composite design of 5 variables with one of center point and 10 axial points, equals 43 different experiments, as one can see from section 5.1.3.

Qian et. al. (2005) [8] did a central composite design of 5 variables to investigate the length of the vortex, but the inlet area was taken as two different variables (the width and the length) and only the cylindrical section of the length was varied. In this thesis both the cylindrical and conical section is a variable, and the inlet area is only one variable.

The coded values used in the design (with a diameter of 0.2 m) can be seen in table 6.4 and the whole setup can be seen in table B.1 in the appendix.

Table 6.4: Coded values

Variable	Low (-1)	Center (0)	High (+1)
D_x/D	0.3	0.4	0.5
$(H - H_c)/D$	1	2	3
H_c/D	2	3.5	5
$(ab)^{0.5}/D$	0.21	0.37	0.53
$ln\ Re$	10.3	14.2	14.9

The low Re models had a uniform grid size in the whole model. The reason for this is that due to the low inlet velocity, the cell size was quite big for the $y+$ value of 30 (7.5 mm), therefor this cell size was used throughout the whole model. A uniform cell size model for low Re was also successfully used by Derksen et. al. [38] in their experiments. The high Re had a near wall layer thickness of 0.1 mm, 3 prism layers of a total thickness of 2 mm and 4.5 mm core.

All simulations was carried out for 10 sec of physical time to ensure that the vortex position was stable. If the vortex ended in the cylindrical tube under the cyclone body, it was noted as the length of the cyclone and not the position in the tube.

6.2.3 Cyclones with wall roughness

Simulations of cylinder-on-cone cyclones with roughness of 0.2 mm was performed to compare with the results in Rødlands (2011) master thesis [16]. For this simulations LES model was used, were the wall roughness can be set by changing the E value (the theoretical background for this value is given in section 5.3) as this is implemented in the wall function.

In earlier experiments conducted at the University of Bergen, a strong influence of wall roughness was seen on the flow rate needed for centralization of the vortex [10], and for the longest tube, it remained on the wall even for extremely high flow rates. A

direct comparison with these experiments was not done, other than using the same wall roughness to see if the trend was the same. In these simulations the Hoffmann cyclone with D_x of 0.075 m was used for better comparison with the previous simulations done in this thesis.

The E value for roughness of 0.2 μm is 1.2. The default value of $E = 9$ corresponds to smooth walls.

Chapter 7

Results and discussion

7.1 Experimental results

Experiments was performed with swirl tubes of different lengths to show the existence of the end of the vortex phenomenon. It is difficult to measure the exact length of the vortex in experiments because the flow has to be visualized, for example by adding more dust or injecting smoke. By doing this the flow conditions are changed and therefor not representable for flow without these interferences.

These experiments was only conducted to show the existence of the EoV phenomenon, and compare with previous results done at the University of Bergen. The length of the vortex is studied more comprehensively with CFD, and not only for purely cylindrical cyclones.

7.1.1 Results of flow rate measurements and pressure transducers

The formation of vortex was studied in three different swirl tube lengths. Pressure was also measured at different depths in the tube, it was then possible to determine where in the cyclone the vortex first attached to the wall and moved downwards. For some of the flow rates where the vortex ended on the wall, it was also tried an increase of flow rate while the pump was still running. The vortex then remained on the wall even for flow rates where it was normally centralized. Only at high flow rates it became centralized.

In the pressure transducer, a voltage is measured and registered in the computer program LabView which gives a output graph for the time span measured. A peak in the graph indicates that the vortex core passes the pressure tap at the given time. In the LabView output the white graph is the measurements and the red graph is a baseline measured above the swirl vanes. When comparing the results with those of Peng et. al. (2005) [5], the images from LabView are inverted. That means a peak in the graph, is a pressure drop, not pressure rise.

Different positions is measured with the same flow rate. This makes it possible to see where and when the vortex passes by, and where there is a stable position, assuming the pressure tap is on one of these positions.

High speed pressure measurements was done to measure the frequency at which the vortex core rotated around when at a stable position on the cyclone wall. This can be seen in figure 7.1, where the frequency can be estimated by counting cycles for a time sequence. In this case the frequency is approximately 42 Hz.
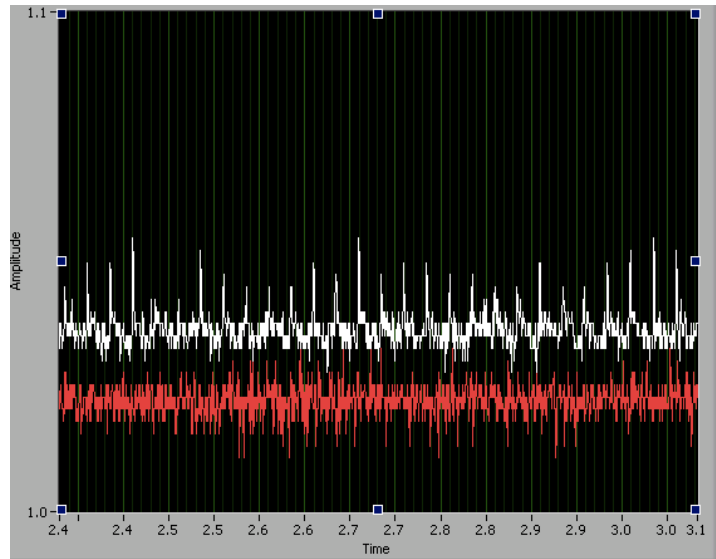
Figure 7.1: Pressure measurements in a 80 cm long swirl tube, the white line is showing the frequency at which the vortex rotates over the pressure transducer at a stable position. The red line is a baseline

When there was a heavy dust loading, the bottom of the tube was coated in dust and one could see the vortex as a ring in moving dust, stabilized in the coated dust.

60 cm swirl tube

The 60 cm swirl tube was the shortest in the experiments. Flow rate measurements showed that centralization of the vortex core happened with flow rates lower than 39.7 m^3/h. See table A.1 in the appendix for all the measurements done on this swirl tube. Meassurements with pressure transducers showed that the vortex core first attached to the wall between 29 and 32 cm from the vanes. The measurements for 78 m^3/h can be seen in figure 7.2.
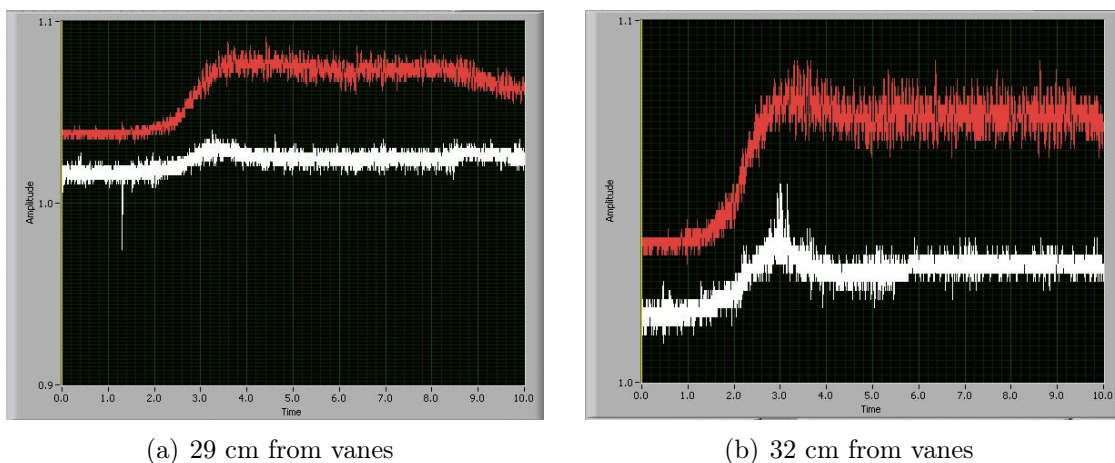
(a) 29 cm from vanes

(b) 32 cm from vanes

Figure 7.2: Measurements of pressure taps positioned 29 cm and 32 cm from swirl vanes at flow rate Q = 72.5 m^3/h in the 60 cm swirl tube.

In figure 7.2 measurements of 10 seconds is done with a flow rate of 72.8 m^3/h. It is observed that the vortex centralizes at this flow rate, but with pressure measurements

at axial positions it is indicated that the vortex bends to the wall between 29 and 32 cm below the vanes, since the vortex passing is not registered in figure 7.2(a), but is registered passing in figure 7.2(b). The same behavior is seen in the tested flow rates 102 and 173 m^3/h, the vortex bent to the wall between 29 and 32 cm from the wall. The LabView output is shown in the Appendix A. This could be an indication of the vortex length being independent of flow rate (inlet velocity).

80 cm swirl tube

Centralization of the vortex core in 80 cm swirl tube was seen with flow rates lower than 58.7 m^3/h.

The results of the flow rate measurements of the 80 cm swirl tube can be seen in table A.2 in the appendix.

(a) 28 cm from vanes

(b) 34 cm from vanes
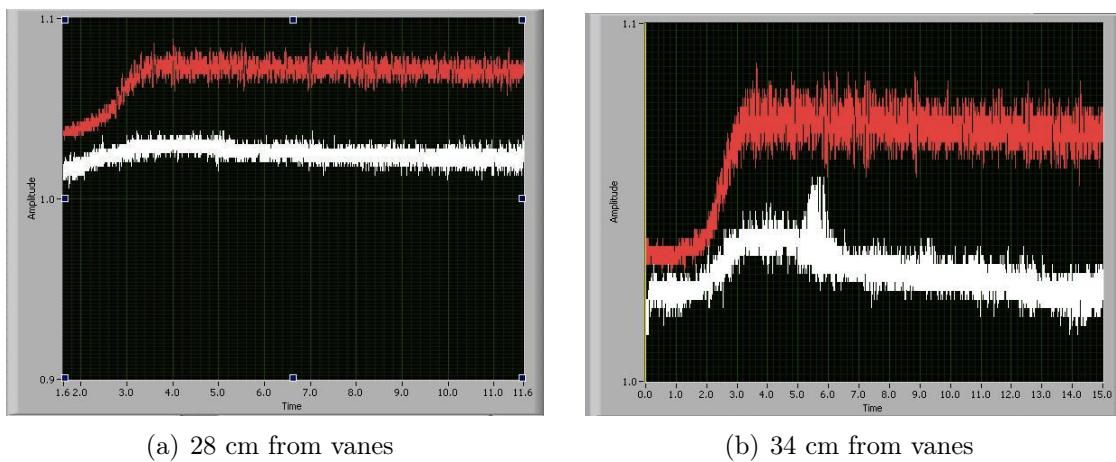
Figure 7.3: Measurements of pressure taps positioned 29 cm and 32 cm from swirl vanes at flow rate Q = 67 m^3/h in the 80 cm swirl tube

In figure 7.3 it can be seen that the vortex core bends to the wall between 28 and 34 cm below the swirl vanes at a flow rate of 67 m^3/h. The same was seen for 70.7 and 156.6 m^3/h.

100 cm swirl tube

Centralization of the vortex core in 100 cm swirl tube was seen with flow rates lower than 85.2 m^3/h. The longer the cyclone is, the higher flow rate is needed to centralize the vortex. The results of the measurements of the 100 cm swirl tube can be seen in table A.3 in the appendix.

Measurements using pressure taps can be seen in figure 7.4. All three cyclone lengths had a vortex core bending to the wall between approximately 28 and 31 cm in the beginning of the measurement period.

Comparison with earlier experiments

New measurements where taken of the flow rate needed for centralization with the same tube lengths as in earlier experiments [15], but with continuous tubes without connections.

(a) 28 cm from vanes   (b) 31 cm from vanes
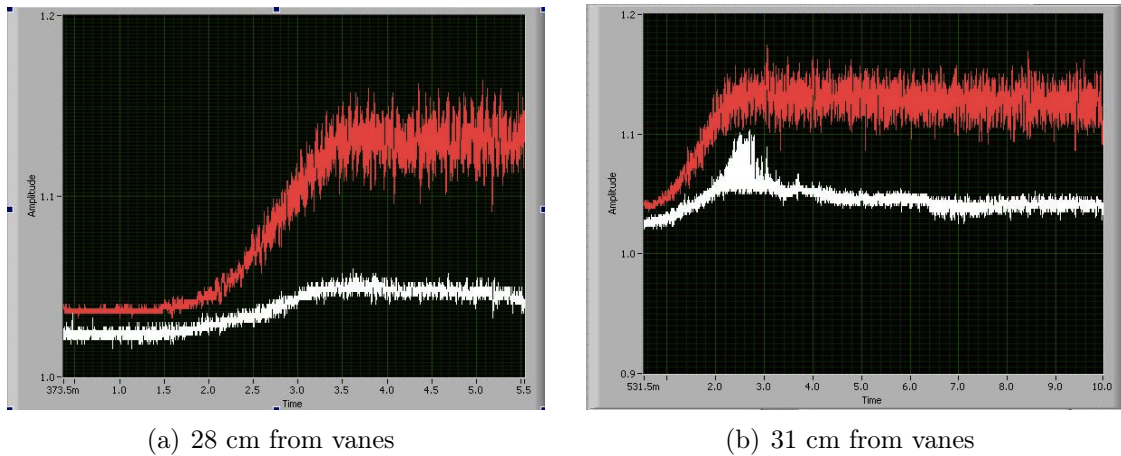
Figure 7.4: Measurements of pressure taps positioned 28 cm and 31 cm from swirl vanes for 10 seconds at flow rate Q = 111.5 m^3/h in the 100 cm swirl tube

As seen in figure 7.5, a tube length made of shorter tubes requires a higher centralization rate than one continuous tube. The values for the earlier experiments are the average of the results from each tube length, because each total tube length was measured with different compositions of shorter tubes.

It seems that the connections has a severe impact on the flow rate needed for centralization, and therefor also the whole flow pattern. There is not a smooth transition between the connected tube parts, and should not be used to study the effect of the length of the cyclone body.
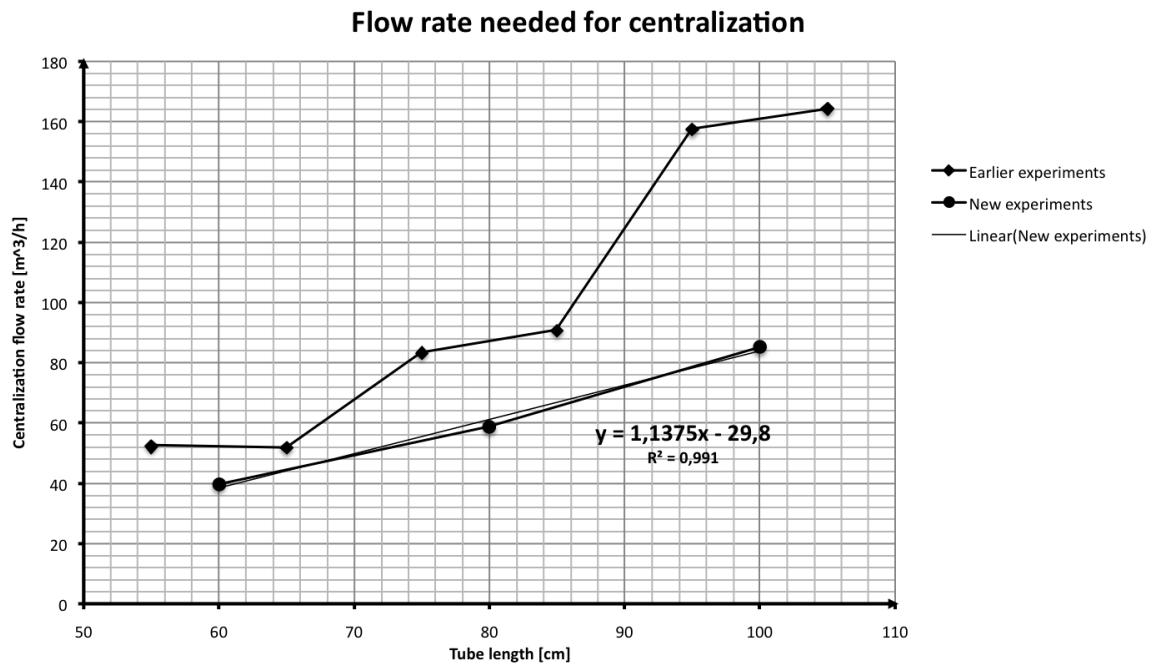
Figure 7.5: Flow rate needed for centralization in continuous tubes (new experiments) and tubes with connections (earlier experiments) and the linear model for the new experiments.

For the new experiments, a close to linear relation is seen. By using linear regression

a trend line can be fitted for the flow rate needed for centralization in terms of cyclone length. The R^2 value, for which 1 is a perfect fit, for this line is 0.991 which shows that this is a good fit. But it is important to notice that outside this range has not been tested, and not for other types of cyclones, and therefor this can not be considered to be true outside the range of these measurements. The experiments with tube with connection where not very close to a linear relation, and a line was therefor not fitted for this. The various slopes between each swirl tube length could be explained by the different number of connection used in the experiment.

7.1.2   Sources of error

A wall that is smooth and have no apparent roughness will still have some roughness which can not be measured. If the pump was restarted to soon, there would still be flow and instability in the tube that would cause error. Too much particles in the tube (for visualizing the vortex) caused the vortex to be more stable at the wall, and harder to centralize. This indicates that surface roughness is important. There are also errors connected to the flow rate measurements and the pump.

7.2   Computational results

A computational model was built to study the length of the vortex in the cylinder-on-cone cyclones. A LES turbulence model was chosen, and after a grid dependency test was performed, a cell size of 4.5 mm was used.

Table 7.1: Courant numbers of different time steps in a 4.5 mm cell and velocity of 10 m/s

Time step	Courant number
0.15 ms	0.375
0.5 ms	1.25
1 ms	2.5

Courant number of approximately 1,5 was used for all simulations. In table 7.1 Courant numbers for different time step with 10 m/s are listed. Since the Courant number is dependent on velocity, time step and cell size the two latter had to be adjusted when changing the velocity.

A two-layer model and a model using the wall functions where tested to see the influence on the vortex length. They gave the same result, and for this purpose it was not necessary to resolve the boundary layer. The computation time for the wall function model was approximately $\frac{1}{4}$ of the time needed for the model resolving the boundary layer.

Four simulations was also performed to test the influence of the prism layers. One was done with equal sized cell on the whole domain, and three with different numbers of layers and thickness, see table 6.1. They where only run for 2 seconds of physical time, and this is not necessarily a stable position, but it was done to see the difference between the models. This shows that using a smaller number and thickness than recommended

can have huge influence on the vortex length. Using no prism layers gave approximately the same result as the two layer zonal and wall function model, showing that the all y+ wall treatment is working. In this case it is probably because the cell size is 4 mm (which is a wall distance of 2 mm from the center of the cell and a y+ of ≈ 70, and this is within the recommended wall y+ value of 30-100).

(a) No prism layers   (b) 2 prism layers

(c) 3 prism layers   (d) 5 prism layers
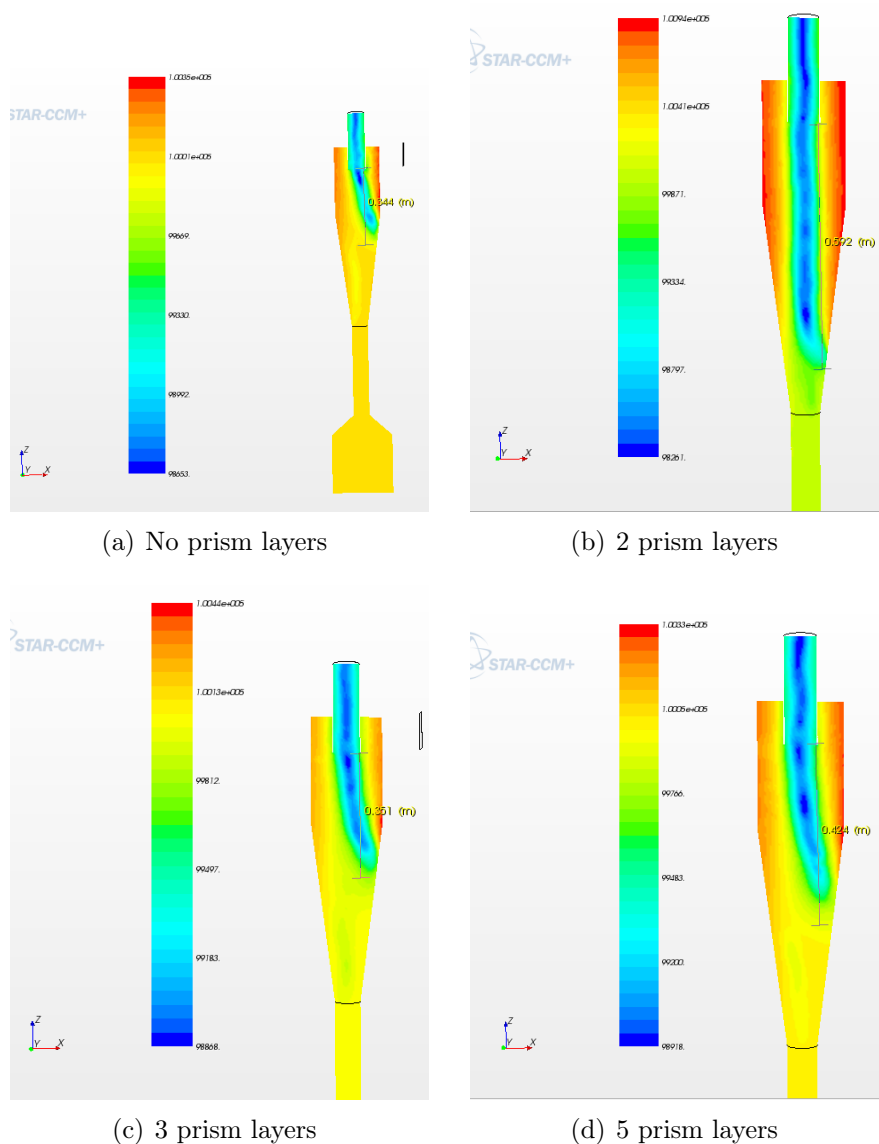
Figure 7.6: Static pressure plots showing vortex length in simulations done with different numbers of prism layers. One with no prism layers and only 4 mm cells, three with wall y+ value = 1 and, total thickness of respectively 0.1 mm, 0.5 mm and 1mm and 4 mm cells in the core region.

As seen in figure 7.6 there is no clear trend for the relationship between the number of prism layers, the thickness of the total layer and the vortex length. The recommended number of prism layers when resolving the boundary layer is 10-20, and the total thickness should exceed the thickness of the boundary layer. This is not the case in any of the simulations and the flow pattern will be influenced by this. This shows the importance of appropriate near wall meshing.

7.2.1   The Hoffmann cyclone

Simulations for cyclones with two different vortex finder diameter was done for comparison with earlier experiments. As expected the simulations gave shorter vortex length than the experiments, probably because of the higher density in the experiments (causing higher Re number). The length of the vortex is not given in cm from the vortex finder diameter, but in coordinates where the dust outlet is 0. This is done because most of the experimental results ended in the cylindrical section below the dust outlet.

The vortex length in the experimental and numerical results follow the same trend, as seen in figure C.2. From approximately 5-15 m/s the vortex length gradually increases with the inlet velocity, from around 15-20 m/s the curve is steeper, and up to 30 m/s the curve flattens out again. This shows clearly that the gas velocity is important. The experimental results have a longer vortex, probably due to the higher density of the gas.
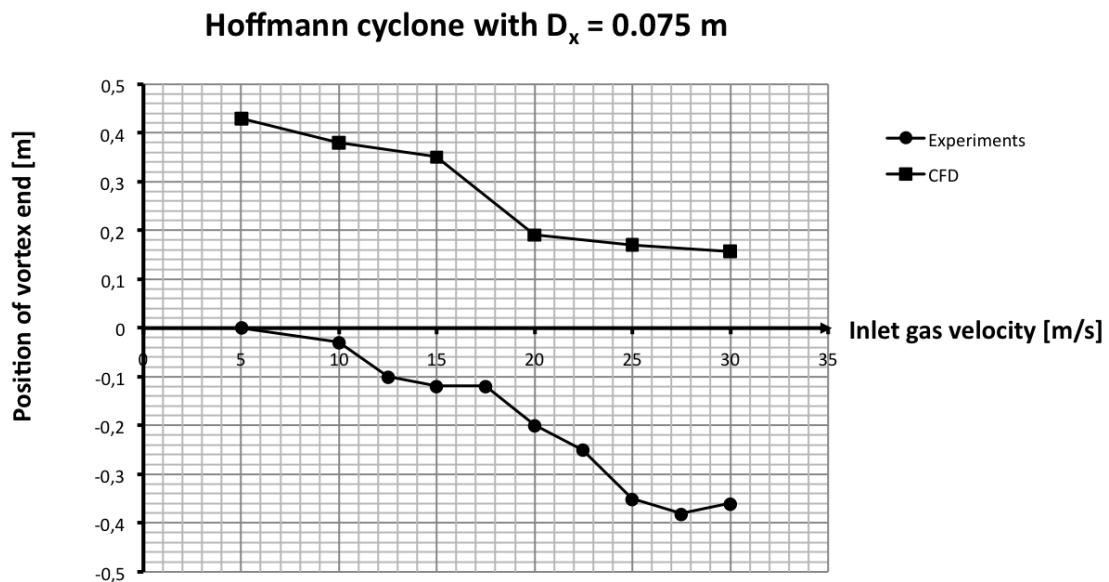
Figure 7.7: CFD results compared to experimental results (obtained from Hoffmanns experiments [3]) of cyclone with 0.075m vortex finder diameter.

When using the existing equations for the vortex length one get the lengths as seen in table 7.2. As seen none of the existing models predicted the length correctly. But the Qian model was qualtatively consistent with the measured lengths, it increased with increasing velocity. The Alexander model is in the same order of magnitude with the only measurement that ended in the cylindrical part. This indicates that the model can be used for cylindrical cyclones with low velocities.

7.2.2   A new model for the natural vortex length

The cyclones with low Re number used several seconds of real time to form a vortex and to be at a stable position at the wall, the cyclones with high Re almost immediately attached to a stable position. This was also seen in the previous experiments, both CFD and experimental.

Table 7.2: Natural vortex lengths for a Hoffmann cyclone with $D_x = 0.075\ m$ with different equation and measured results

Equation	2.21	2.23	2.24	2.25	
v	Alexander	Bryant	Zhongli	Qian	Measured
N/A	0.37	3.8	1.9		
5				0.57	0.27
10				0.63	0.32
15				0.67	0.35
20				0.69	0.51
25				0.71	0.53
30				0.72	0.54

43 simulations of a central composite design was performed to make a new model for the vortex length.

Some observations where made during the simulations:

- In the simulations with low Re the vortex used some time to form inside the cyclone body.

- For the simulations with high Re the vortex formed almost immediately both for centralized vortex and vortex that attached to the wall.

- All the shorter cyclones experienced a centralized vortex, in the most of the longer cyclones the EoV phenomenon occurred.

- A longer section of conical region seemed destabilizing on the vortex and caused shorter natural vortex length.

.

Surface plots for two and two variables are plotted against the averaged vortex length for the experiments in question. All the surface plots can be seen in figure 7.8 and 7.9.

(a) D_x/D and $(ab)^{0.5}/D$

(b) D_x/D and $(H-H_c)/D$

(c) D_x/D and H_c/D

(d) D_x/D and $\ln Re$

(e) $H-H_c/D$ and $(ab)^{0.5}/D$

(f) $(H-H_c)/D$ and H_c/D
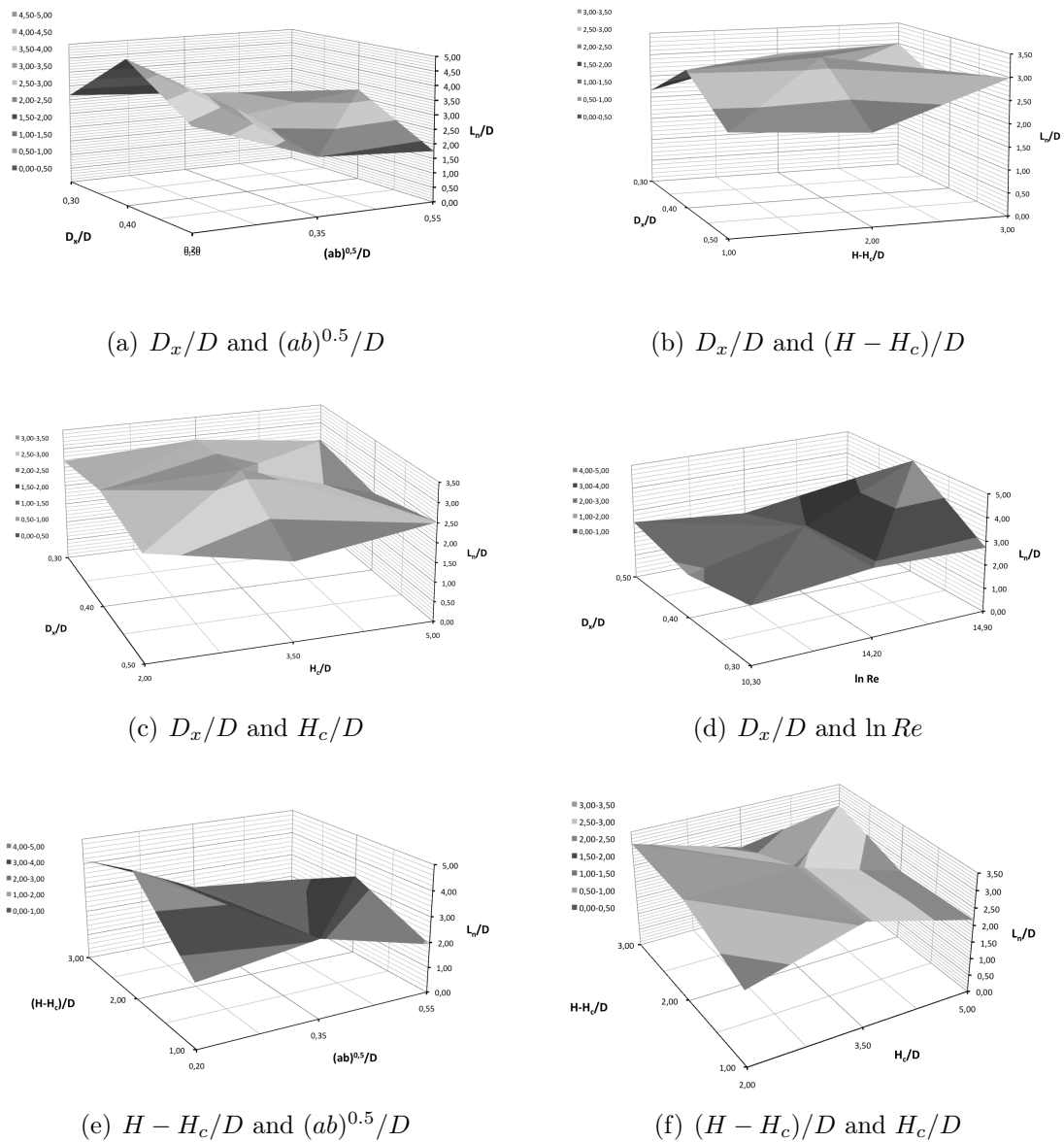
Figure 7.8: Surface plots of the central composite design variables against the averaged response for the two variables in each plot. The variables are made dimensionless

In figure 7.8(a) the factors D_x/D and $(ab)^{0,5}/D$ are plotted against L_n/D. A clear trend can be seen that the L_n/D increase with decreasing inlet area. This is consistent with Alexanders equation. The D_x/D seems to have a maximum at the center point.

In figure 7.8(b) it is seen that the variation of L_n/D is not substantial. But the maximum at the center point for D_x/D is also seen here, although is seems to have a minimum at the center point at the highest value of $(H-H_c)/D$. $(H-H_c)/D$ also have minimum at the center point with the largest vortex finder. This interaction is accounted for in the model of Qian.

From figure 7.8(c) it is seen the variation of L_n/D is not very substantial here either. One would expect the H_c/D to have a larger influence because of the instability a conical part creates as opposed to a purely cylindrical part. The conical part is not included in any previous models, but even if it is not a huge affect, it still influence the length of the

vortex.

The inlet velocity, in terms of $\ln Re$, has a clear impact on the vortex length as seen in figure 7.8(d). The L_n/D also has large values for the center point of the D_x/D with the highest inlet velocities. But with the lowest value of inlet velocity there is a minimum at the center point. Both in Hoffmanns experiments [3] and Qians [8] experienced longer L_n/D with increasing D_x/D until it reached a maximum and became shorter after this. This is consistent with the results in the experiments of this thesis, but it seems like the interactions with other variables are also important.

In figure 7.8(e) the values of L_n/D is, as expected, high for low values of $(ab)^{0.5}/D$, but an interesting feature is that for the center points of both variables there is a minimum. Only Qians equation has a term considering the length of the cyclone, but purely cylindrical, this can be compared with the factor $(H - H_c)/D$, the cylindrical part, and these are qualitatively consistent with each other.

Figure 7.8(f) shows that $(H - H_c)/D$ and H_c/D has an about equal amount of influence, which indicates that the length of the cyclone body is important. It also shows that a large conical section cause an slight decease in L_n/D which is consistent with the theory that the cyclone length can not be made arbitrary long and that a conical section decreases the vortex length. This is not included in any of the previous models.

(a) $H - H_c/D$ and $\ln Re$

(b) H_c/D and $(ab)^{0.5}/D$

(c) H_c/D and $\ln Re$

(d) $(ab)^{0.5}/D$ and $\ln Re$
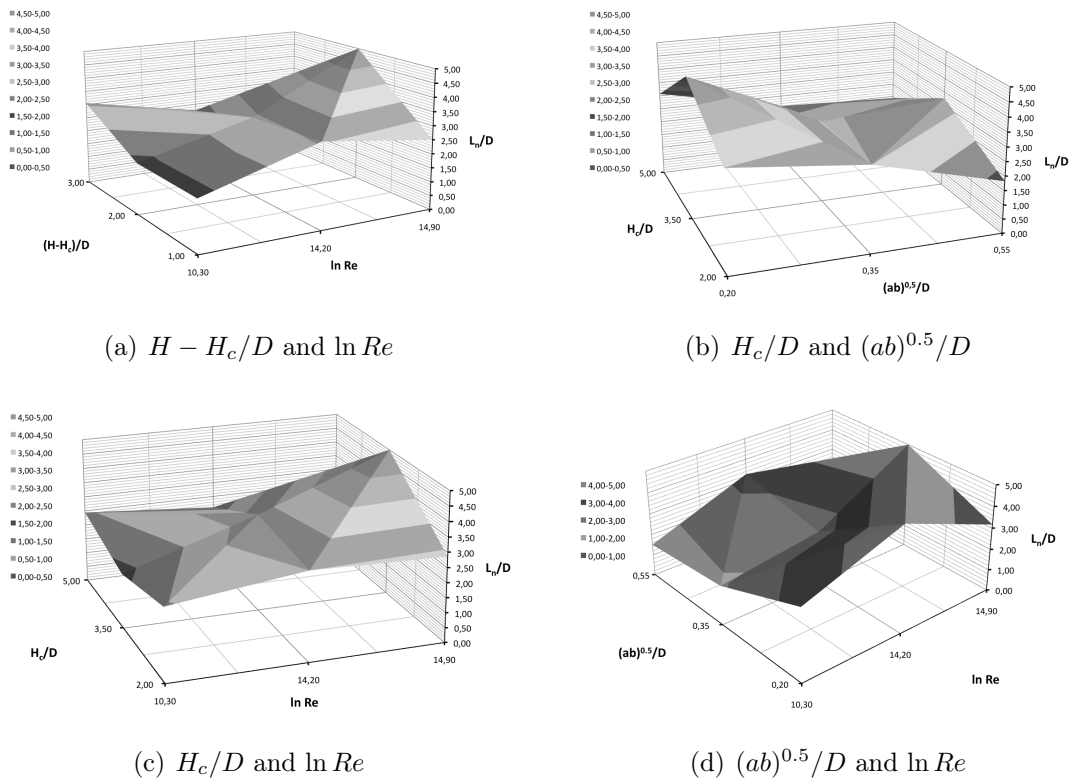
Figure 7.9: Surface plots of the central composite design variables against the averaged response for the two variables in each plot. The variables are made dimensionless

In figure 7.9(a) the trend for $\ln Re$ is shown here as in the other plots, but it also shows variation that can not be described by a second order model. The variation of L_n/D with $H - H_c/D$ is smaller than for $\ln Re$.

In figure 7.9(b) $(ab)^{0.5}/D$ has a saddle point for the center point values, but the trend

here is that the vortex length decreases with increasing inlet area. There is an increase in length with increasing conical section, until it reaches maximum at the center point and decrease after this. This is not taken into account in any other models than the Qian model.

Figure 7.9(d) does not show a clear trend for $(ab)^{0.5}/D$ and $\ln Re$. A minimum is seen at the center point for both variables, but there are also minimums at high values of $\ln Re$ and low value of inlet area. The decrease of vortex length with increase of inlet area is consistent with the equations of Bryant and Zhongli.

A second order model was found by performing multiple regression in the commercial software SPSS. The estimates of the regression coefficients can be seen in the appendix in figure D.2 together with statistics concerning the model. By looking at the significance of the of the coefficients, the two-factor interactions $(D_x/D) * ((H - H_c)/D)$ and $(D_x/D) * (H_c/D)$ can be considered insignificant and is therefor taken out of the equation. It is assumed that three-factor is always insignificant and where not considered in the analysis at all. This gives the equation for the new model:

$$
\begin{aligned}
\frac{L_n}{D} = {} & 12.05 + 59.55 \left(\frac{D_x}{D} \right) - 68.06 \left(\frac{D_x}{D} \right)^2 + 4.69 \left(\frac{H - H_c}{D} \right) \\
& - 0.47 \left(\frac{H - H_c}{D} \right)^2 + 1.91 \left(\frac{H_c}{D} \right) - 0.252 \left(\frac{H_c}{D} \right)^2 - 32.37 \left(\frac{(ab)^{0.5}}{D} \right) \\
& + 36.61 \left(\frac{(ab)^{0.5}}{D} \right)^2 - 3.75 \left(\ln Re \right) + 0.16 \left(\ln Re \right)^2 - 6.73 \left(\frac{D_x}{D} \right) \left(\frac{(ab)^{0.5}}{D} \right) \\
& - 0.22 \left(\frac{D_x}{D} \right) \left(\ln Re \right) - 0.49 \left(\frac{H - H_c}{D} \right) \left(\frac{H_c}{D} \right) + 2.56 \left(\frac{H - H_c}{D} \right) \left(\frac{(ab)^{0.5}}{D} \right) \\
& - 0.10 \left(\frac{H - H_c}{D} \right) \left(\ln Re \right) + 0.51 \left(\frac{H_c}{D} \right) \left(\frac{(ab)^{0.5}}{D} \right) - 0.03 \left(\frac{H_c}{D} \right) \left(\ln Re \right) \\
& + 0.54 \left(\frac{(ab)^{0.5}}{D} \right) \left(\ln Re \right)
\end{aligned}
$$
(7.1)

The model has a R^2-value of 0.832 which is a fairly good fit. Without the interaction terms the R^2-value is 0.59, calculated using multiple regression in Microsoft Excel, which suggest that interactions plays an important part. Both the interaction $((H - H_c/)D) * (((ab)^{0.5})/D)$ and $(((ab)^{0.5})/D) * (\ln Re)$ has a great impact on the length of the vortex according to the model.

One simulation to test if the length could be predicted was also performed. This cyclone was made with dimensions and Re within the range of which the model was made. The dimensions of the cyclone where: $D_x = 0.07$, $H - H_c = 0.50$, $H_c = 0.65$ and $(ab)^0.5 = 0.056$. The operational condition, $Re = 1.00 \times 10^5$. L_n in this simulation was 0.408 m, and the predicted value was 0.64 m. The predicted value is higher than the measured, but this can be explained by the accuracy of the regression model.

The measured values of the length of the vortex where plotter against the predicted value to show the predictability of the model. The plot can be seen in figure 7.10.

Some of the error in the model is probably due to the fact that it is fitted to a
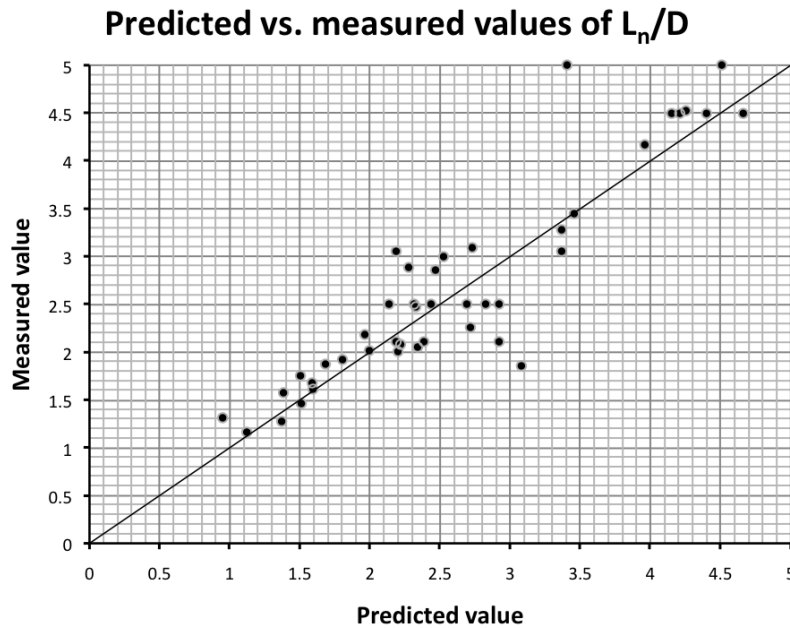
Figure 7.10: Normal probability plot of predicted versus measured value of the vortex length. This shows the predictability of the model.

second order polynomial, and not a higher order. From the surface plots, where several of them have saddle points or two maximum/minimum points, it looks like a third order model should be considered. This can be done by adding five third-order terms to the equation, and should be investigated in further work. An interesting feature here is that the velocity term, $\ln Re$, has ha negative sign, even if the trend of all the surface plots, and earlier experiments, show that higher velocity gives a higher value of L_n/D. This is probably due to the best fit of the second order regression model, which has a R^2 value of only 0.8.

The total length of the cyclone is not taken into account either, it is given by the cylindrical and the conical part, but they are regarded as independent variables, and in some cases one could get a L_n/D that is longer than the cyclone length. When doing measurements, if the vortex ended somewhere under the cyclone body, only the length of the body was used, because this is a centralized vortex and the whole separation space is utilized. Therefor one should not have gotten vortex lengths that are longer than the cyclone body. This could perhaps be accounted for by using a cylindrical/conical part ratio and the cone angle. In the experiments performed by Qian the turning point for the vortex was in the cylindrical tube under the cyclone body, and therefor a the EoV phenomenon was not present [8]. But exactly where it ends underneath the cyclone body is not very useful for the cyclone designer, since it is when the EoV is present the separation space is shortened.

Even if the regression model is not as accurate as one could want, the computational results sheds light on the importance of including other geometrical parts, as the conical section and cylindrical section, and the Reynolds number in a model for the vortex length.

7.2.3   Cyclones with wall roughness

Three simulations with different inlet velocities was performed on the Hoffmann cyclone with $D_x = 0.075$ m. To each of the simulations a wall surface roughness of 0.2 mm was applied by changing the E-value of the blended wall function from default value 9 to 1.2. The results of this was compared to the simulations of the same cyclone but with smooth walls. The position of the EoV is plotted in figure 7.11.

Position of EoV in a Hoffmann cyclone with and without roughness
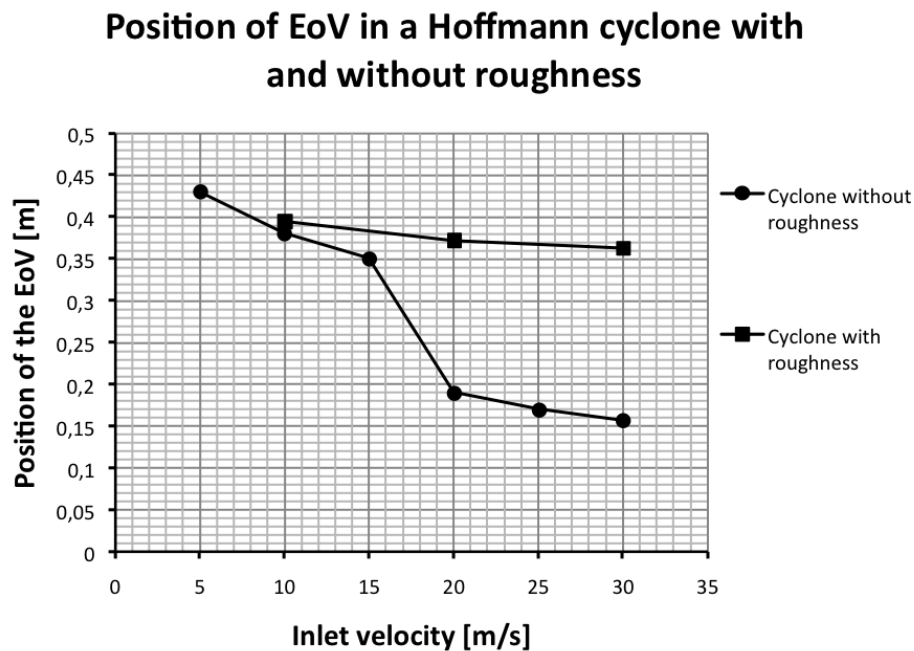
Figure 7.11: Normal probability plot of predicted versus measured value of the vortex length. This shows the predictability of the model.

As for the other simulations of the Hoffmann cyclone, the length of the vortex is not plotted, but the position of the EoV, for easier comparison with those experiments. As seen in the plot, the length of the vortex with the surface roughness seems close to independent of the velocity. This implies that the roughness has a large influence on the flow pattern in the cyclone, and is in agreement with what was found in previous studies [10],[16]. Only one roughness height was tested, and it could be interesting to see how the length of the vortex changed with the roughness also, and this should be further investigated.

7.2.4   Sources of error

In CFD simulations there can be discretization errors, modeling errors and iteration errors. But since the length of the vortex was measured manually, there is also an experimental error. This is expected to be smaller than in actual physical experiments since the measurements are on an image and not a moving vortex measured from outside of the cyclone. The modeling error can be difficult to quantify. Comparing with experimental results gave the same trend, but since the density of the gas, with smoke added, in the experiments was unknown they can not be fully compared. Also the initial pressure and temperature could be different in the experiments than in the simulations.

A grid dependency test was performed to ensure that the solution was independent of the grid size. Using a large cell size would result in a discretization error. Cell sizes of 6 mm, 5mm, 4.5 mm, 4 mm and 3.5 mm was performed, and it was found that the velocity profile over a plane section of the whole cyclone body did not change very much for cell sizes lower than 4.5 mm.

Different time step was also tested. As seen in figure 7.12 0.001 s did not show the behavior of the axial velocity as seen in figure 2.10(a). 0.0005 s corresponds to a Courant number of 1.11 with a cell size of 4.5 mm. In literature it is recommended a value below 1, but experiments has shown that values up to 2 does not show much worse convergence behavior, and therefor this was used.

(a) 0.001 s   (b) 0.0005 s
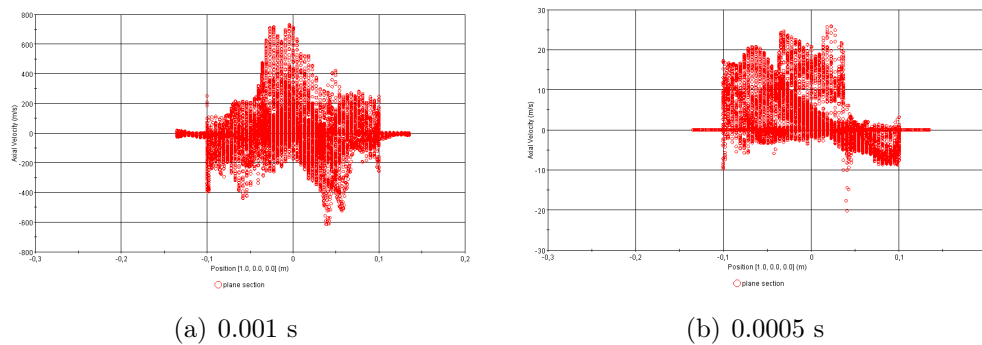
Figure 7.12: Axial velocity profile in a plane section of the whole cyclone body for two different time steps

As seen in figure 7.13, the solution showed convergence behavior after only a few iterations, but if more iterations where used one could get lower values of the residuals. But this is only important if the solution changes.
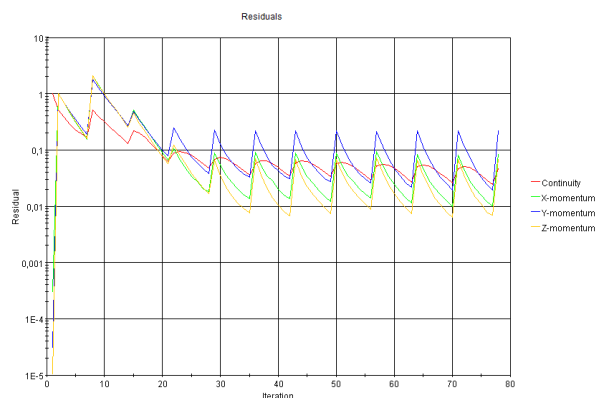
Figure 7.13: Residual plot of the solution converging on each time step

7.3   Summary of the results and further discussion

In this thesis, the end of vortex phenomenon, EoV, was studied experimentally in swirl tubes. The flow rate needed for the vortex core to centralize in the cyclone body could be measured with a venturi flow meter. This was done for swirl tubes with tube length of 60, 80 of 100 cm. In earlier studies the flow rate needed for centralization was measured

for tubes constructed with smaller tube length. The connections between the tubes was seen to have a high influence on the flow, giving a higher centralization flow rate, and a continuous tube should be used. A physical explanation for this is that the tubes connections causes to wall to be uneven, or very rough compared to the rest that is smooth, and because of this the vortex length is shorter. The new measurements showed that the flow rate needed for centralization is higher for longer cyclones, with a close to linear correlation between the flow rate and length of the tube. For flow rates lower than the one needed for centralization, the vortex core remained on the wall at stable positions. The length of the vortex was not measured in these experiments. To visualize the vortex, a heavy dust load had to be introduced to the flow and this influenced the flow pattern. The vortex end could then be seen as a ring in the dust on the wall of the cyclone, but this is not the vortex length for this flow rate because of the increased roughness due to the particles on the cyclone wall.

Pressure transducers on the cyclone body made it possible to do pressure measurements as the vortex core descended in the cyclone body. A sudden drop in pressure was seen when the core passed the transducer. The recording of measurements started when the pump was started. Measurements was done for different distances from the swirl vanes, and the vortex attached between 29 and 32 cm from the vanes in all cases. This method was not used to measure the length of the vortex either, because the transducers where positioned 3 cm apart, and if the vortex ended between two the exact length could not be measured.

Computational fluid dynamics, CFD, simulations where conducted on cylinder-on-cone cyclones in order to study the length of the vortex inside the cyclone body. The dimensions where the same as Hoffmann et. al. [3] used in their experiments, and the numerical results where compared with the experimental. Good agreement was found between the earlier experiments and the simulations performed. In the CFD simulations the vortex length was shorter than in the experiment. This was expected since in the experiments smoke was added to the flow for visualization causing a higher density of the flow.

By using response surface methodology a new model for vortex length, based on Re number, length of conical section, length of cylindrical section, D_x/D and inlet area, was made by fitting a second order polynomial to the measured values of the central composite design. This showed that not only the main effects where important, but also most of the interactions. Especially the interaction between the cylindrical section and the inlet area, was important. The vortex length decreased with a higher value of the sum of these two. According to the regression model, the main effects of the cylindrical part and the inlet area are the most important.

Comparing the numerical results with the second order regression model there is a correlation, but the effects of the variables could not be fully described with second order polynomials. A higher order term should be used, because the results of the simulations shows that is is a complex problem. When plotting the variables against the results the surfaces had saddle points or more than one maximum/minimum, which indicates a third or even a forth order polynomial. None of the previous models included the conical part of the cyclone. The results in this thesis showed that the conical part is not the highest influence, but it is a significant effect. Is therefor important to include as a parameter when constructing a model for the vortex length.

The influence of wall roughness on cylinder-on-cone cyclones was also modeled using

CFD simulations. It was found that the natural vortex length is decreased by surface roughness and this effect is also increased by the inlet velocity.

Chapter 8

Conclusion and outlook

8.1 Conclusion

Experiments was conducted on swirl tubes, and the different flow rate needed for centralization of the vortex core was found. A linear correlation between the centralization flow rate and swirl tube length was found. Measurements done with pressure transducers showed where the vortex first bent to the wall, and made is possible to count the frequency of the rotations of the vortex core.

The conclusion of the numerical results on the length of the vortex is listed as follows:

- Higher velocities gives an increase in the length of the vortex.

- The longer cyclones more often had an occurring vortex end remaining on the wall of the cyclone.

- Smaller inlets increased the vortex length.

- The length of the vortex increases with the size of the vortex finder diameter up to a certain point, and after this it decreases.

- An increase in the cylindrical part of the cyclone body gives an increase in the length of the vortex.

- An increase in conical section increases the vortex length up to a certain point, and decreases the length after this.

- The interactions between the variables are very important factors, and therefor a higher order polynomial should be used to describe a model for the vortex length.

- Higher surface roughness gives a decrease in the length of the vortex.

A new model for the vortex length was presented, but due to some lack of fit more work should be done on this.

8.2   Outlook

When performing experimental work on the length of the vortex in gas cyclones, there is challenges when trying to visualize the vortex. In a hydrocyclone the core is visual because of the gas vortex. Peng et. al. [5] used stroboscope for visualization, and this seems like a good alternative since this does not influence the flow pattern. If a colored gas or smoke with known density could be used, it would be easier to study the gas flow without any interferences or limitations with regards to position. But it is subject to experimental errors.

Further work using the pressure measurements with flow rates where the vortex core is at a stable position at the wall should, also be conducted, and which factors influence vortex core remaining at the wall. But using pressure transducers limits the measurements to the position of the transducer.

CFD simulations is therefor a good supplement and alternative to experimental measurements. As the technology advance one can make more realistic models to simulate the complex flow of the vortex. In the CFD experiments in this theses the vortex did not form for some of the geometries and low inlet velocities. It would be interesting to find out at which size of different geometrical parameters the vortex will not form. Another study that could be interesting is to investigate the effect if inlet width and hight in cylinder-on-cone cyclones, in this thesis only the inlet area was considered. Previous work has shown that the width and height could be important, and this could be introduced to the model as to different parameters. The relationship between cylindrical/conical part and cone angle is also something that needs to be further studied. Previous research has been mostly about cylindrical cyclones.

Only three velocities was tested for the surface roughness. Although roughness is not a design parameter, one could do a response surface design with roughness as a parameter to make a new model or at least investigate the roughness further with other, higher, velocities. It is clear that roughness has a great impact on the flow pattern, this was also confirmed in this thesis.

Appendix A

Experimental results

A.1 Experimental results for the 60 cm swirl tube

No comment in the "Observations"-field in the tables means that the vortex has not been centralized, even after running a long time.

Table A.1: Measurements of 60 cm cyclone

Flowrate $[m^3/h]$	Observations
22.4	
26.5	
29.9	
30	
32	
34.1	
37.2	Centralized after 3 sec. Pump restarted to soon.
37.9	
38.3	
39.4	
39.7	Centralized after 35 sec.
39.8	Centralized after 23 sec.
40.2	Centralized after 30 sec.
40.9	Centralized after 20 sec.
41.5	Centralized after 19 sec.
66.2	Centralized after 1.5 sec.

A.2   Experimental results for the 80 cm swirl tube

Table A.2: Measurements of 80 cm cyclone

Flowrate [m^3/h]	Observations
36.2	
55.7	
58.7	Centralized after 43 sec.
67	Centralized after 17 sec.
70.7	Centralized after 18 sec.
71.4	Centralized (time not measured)
74.7	Centralized after 17 sec.
156.6	Centralized after 3 sec.

A.3   Experimental results for the 100 cm swirl tube

Table A.3: Measurements of 100 cm cyclone

Flowrate [m^3/h]	Observations
57.9	
68.8	
85.2	Centralized after 53 sec.
90.2	Centralized after 45 sec.
111.5	Centralized after12 sec.

Appendix B

Central composite design

Table B.1: Central composite design of 43 experiments, where + = high value, 0 = center point and - = low value.

Ex. no	D_x/D	$(H-H_c)/D$	H_c/D	$(ab)^{0.5}/D$	Re
1	-	-	-	-	-
2	+	-	-	-	-
3	-	+	-	-	-
4	+	+	-	-	-
5	-	-	+	-	-
6	+	-	+	-	-
7	-	+	+	-	-
8	+	+	+	-	-
9	-	-	-	+	-
10	+	-	-	+	-
11	-	+	-	+	-
12	+	+	-	+	-
13	-	-	+	+	-
14	+	-	+	+	-
15	-	+	+	+	-
16	+	+	+	+	-
17	-	-	-	-	+
18	+	-	-	-	+
19	-	+	-	-	+
20	+	+	-	-	+
21	-	-	+	-	+
22	+	-	+	-	+
23	-	+	+	-	+
24	+	+	+	-	+
25	-	-	-	+	+
26	+	-	-	+	+
27	-	+	-	+	+
28	+	+	-	+	+
29	-	-	+	+	+
30	+	-	+	+	+
31	-	+	+	+	+
32	+	+	+	+	+
33	0	0	0	0	0
34	-	0	0	0	0
35	+	0	0	0	0
36	0	-	0	0	0
37	0	+	0	0	0
38	0	0	-	0	0
39	0	0	+	0	0
40	0	0	0	-	0
41	0	0	0	+	0
42	0	0	0	0	-
43	0	0	0	0	+

Appendix C

Computational results

C.1 Hoffmann cyclone

(a) 5 m/s (b) 10m/s (c) 15m/s (d) 20m/s

(e) 25m/s (f) 30m/s
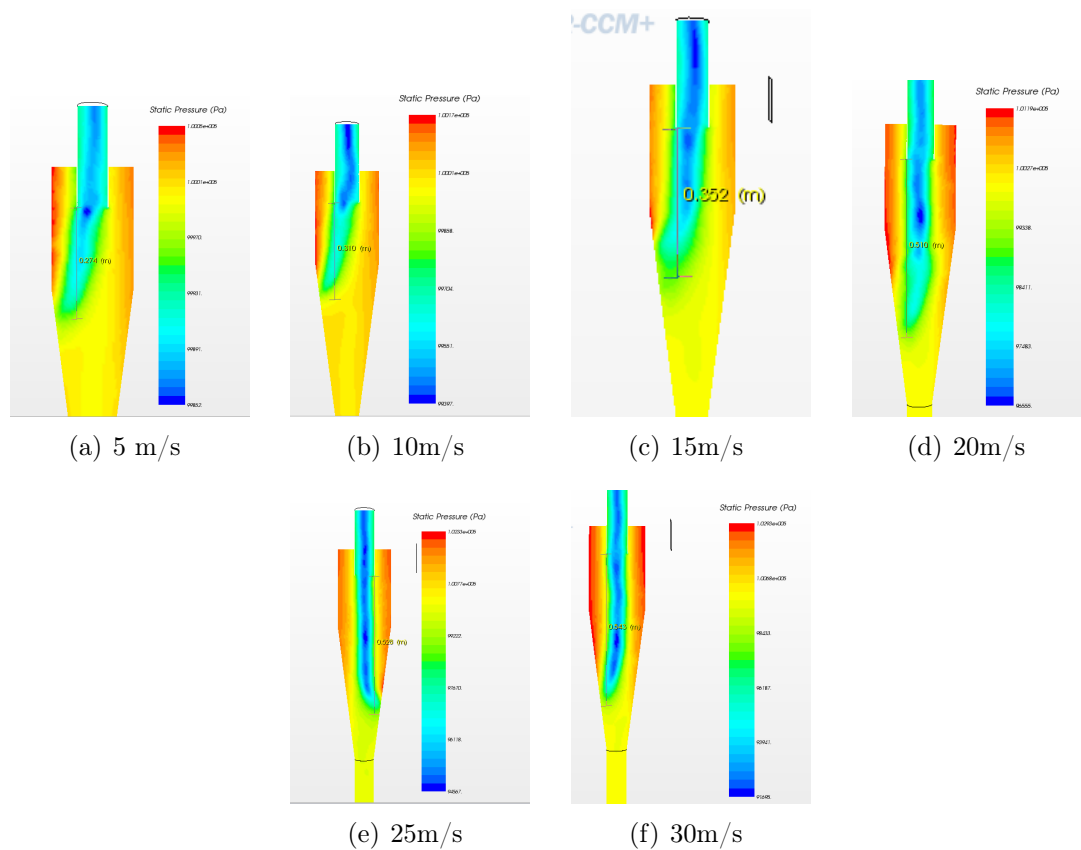
Figure C.1: CFD simulations of a Stairmand HE cyclone with vortex finder diameter 0.075 m. The length of the vortex is indicated on each of the simulations at different inlet velocities

C.2 Central composite design

The results and actual values of all 43 simulations can be seen in table C.1.

Table C.1: Central composite design of 5 variables at 3 levels, and results

Ex. no	D_x/D	$(H-H_c)/D$	H_c/D	$(ab)^{0.5}/D$	ln Re	L_n/D
1	0.30	1.00	2.00	0.20	10.30	2.50
2	0.50	1.00	2.00	0.20	10.30	2.50
3	0.30	3.00	2.00	0.20	10.30	4.50
4	0.50	3.00	2.00	0.20	10.30	4.50
5	0.30	1.00	5.00	0.20	10.30	2.02
6	0.50	1.00	5.00	0.20	10.30	2.48
7	0.30	3.00	5.00	0.20	10.30	4.17
8	0.50	3.00	5.00	0.20	10.30	4.53
9	0.30	1.00	2.00	0.55	10.30	1.17
10	0.50	1.00	2.00	0.55	10.30	1.32
11	0.30	3.00	2.00	0.55	10.30	1.62
12	0.50	3.00	2.00	0.55	10.30	1.58
13	0.30	1.00	5.00	0.55	10.30	1.47
14	0.50	1.00	5.00	0.55	10.30	1.28
15	0.30	3.00	5.00	0.55	10.30	1.88
16	0.50	3.00	5.00	0.55	10.30	1.75
17	0.30	1.00	2.00	0.20	14.90	2.50
18	0.50	1.00	2.00	0.20	14.90	2.50
19	0.30	3.00	2.00	0.20	14.90	4.50
20	0.50	3.00	2.00	0.20	14.90	4.50
21	0.30	1.00	5.00	0.20	14.90	2.06
22	0.50	1.00	5.00	0.20	14.90	2.86
23	0.30	3.00	5.00	0.20	14.90	3.05
24	0.50	3.00	5.00	0.20	14.90	3.45
25	0.30	1.00	2.00	0.55	14.90	2.50
26	0.50	1.00	2.00	0.55	14.90	2.50
27	0.30	3.00	2.00	0.55	14.90	2.08
28	0.50	3.00	2.00	0.55	14.90	1.92
29	0.30	1.00	5.00	0.55	14.90	3.10
30	0.50	1.00	5.00	0.55	14.90	2.11
31	0.30	3.00	5.00	0.55	14.90	2.18
32	0.50	3.00	5.00	0.55	14.90	1.68
33	0.40	2.00	3.50	0.35	14.20	2.11
34	0.30	2.00	3.50	0.35	14.20	2.88
35	0.50	2.00	3.50	0.35	14.20	2.00
36	0.40	1.00	3.50	0.35	14.20	3.05
37	0.40	3.00	3.50	0.35	14.20	2.26
38	0.40	2.00	2.00	0.35	14.20	3.00
39	0.40	2.00	5.00	0.35	14.20	2.11
40	0.40	2.00	3.50	0.20	14.20	5.00
41	0.40	2.00	3.50	0.55	14.20	3.28
42	0.40	2.00	3.50	0.35	10.30	1.85
43	0.40	2.00	3.50	0.35	14.90	5.00

C.3   Roughness

(a) 10 m/s   (b) 20m/s   (c) 30m/s
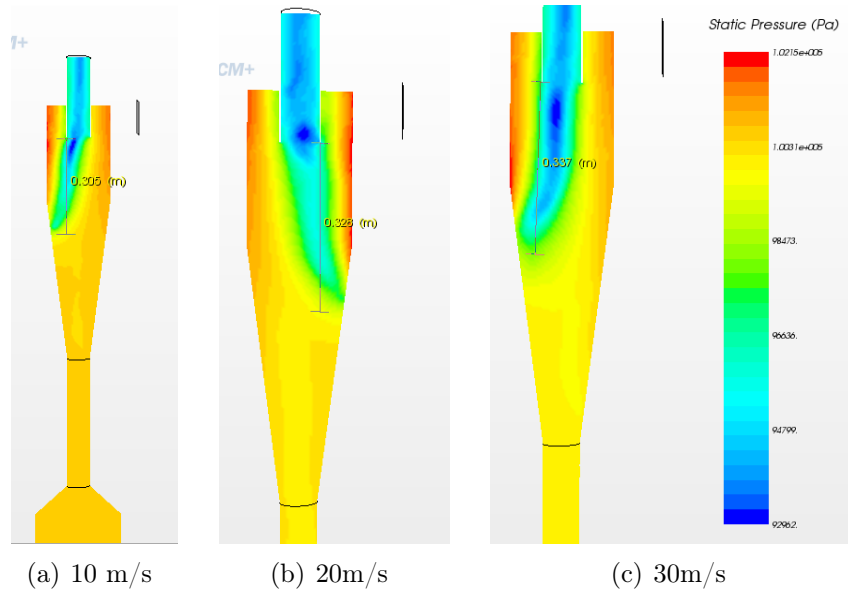
Figure C.2: CFD simulations of a Stairmand HE cyclone with vortex finder diameter 0.075 m with wall roughness of 0.2 mm. The length of the vortex is indicated on each of the simulations at different inlet velocities

Appendix D

Statistics for the computational results

D.1 ANOVA for the results of the new model

An analysis of variance (ANOVA), is an analysis to determine of the factors in an experiment are significantly different [50]. The interactions between the factors is also a part of the regression model. There are different elects in an ANOVA. The sum of squares is given by:

$$
\begin{aligned}
SST &= SSR + SSE \\
SST &= \sum_{i=1}^{n} (y_i - \overline{y}) \qquad \text{Total corrected sum of squares of y} \\
SSR &= \sum_{i=1}^{n} (\widehat{y_i} - \overline{y})^2 \qquad \text{Regression sum of squares} \\
SSE &= \sum_{i=1}^{n} (\overline{y} - \widehat{y_i})^2 \qquad \text{Error sum of squares}
\end{aligned}
\tag{D.1}
$$

Sum of squares reflect the amount of variation within the y-values of the regression model and the error, which is the difference of the predicted values from the measured [45]. The mean square is the sum of squares divided by the degrees of freedom, for the regression it is the number of factors in the model. The F-value is the sum of squares divided by the variance, and is used to perform a F-test, which can decide if the variances are significantly different from each other.

ANOVA^a

Model		Sum of Squares	df	Mean Square	F	Sig.
1	Regression	40.162	20	2.008	5.447	.000^b
	Residual	8.110	22	.369		
	Total	48.273	42			

a. Dependent Variable: Ln/D

b. Predictors: (Constant), ((ab)0.5/D)*(ln Re), ((H–Hc)/D)*(Hc/D), Dx/D, ln Re, (Hc/D)^2, ((H–Hc)/D)*((ab)0.5/D), (Dx/D)*((H–Hc)/D), ((Hc)/D)*((ab)0.5/D), (Dx/D)*((ab)0.5/D), ((H–Hc)/D)*(ln Re), (Dx/D)*(Hc/D), (Hc/D)*(ln Re), ((H–Hc)/D)^2, (ab)/D^2, (Dx/D)*(ln Re), (H–Hc)/D, ((ab)^0.5)/D, Hc/D, (Dx/D)^2, (ln Re)^2

Figure D.1: Resuls the ANOVA for the variables of the central composite design to investigate the influence of the natural vortex length. Performed with software SPSS.

The ANOVA-table for the regression model for the model of the vortex length can be seen in figure D.1. The commercial software SPSS is used to calculate the values in the ANOVA table. The low significance value, some times reffered to as the probability-,

or p-, value. indicate that the calculation data are fitted well by the model, with more than 95 % confidence level.

The regression coefficients are listed in figure D.2. Together with the standard error, standardized coefficients, t-value and the significance. The lower the value of the significance, the more significant is the influence of the factor to the model. When the standard error is larger, the significance approaches unity and the influence of the factor can be seen as insignificant to the model. If the significance is higher than 0.5, the influence is lower than 95 % confidence level. The t-value is a standard error ratio, which decreases with increasing significance.

Model		Unstandardized Coefficients		Standardized Coefficients		
		B	Std. Error	Beta	t	Sig.
1	(Constant)	12.045	20.637		.584	.565
	Dx/D	59.548	31.818	4.998	1.872	.075
	(Dx/D)^2	-68.057	38.748	-4.577	-1.756	.093
	(H-Hc)/D	4.693	1.748	3.938	2.685	.014
	((H-Hc)/D)^2	-.468	.387	-1.582	-1.208	.240
	Hc/D	1.905	1.318	2.398	1.445	.162
	(Hc/D)^2	-.252	.172	-2.236	-1.466	.157
	((ab)^0.5)/D	-32.373	10.690	-4.765	-3.028	.006
	(ab)/D^2	36.611	12.927	4.091	2.832	.010
	ln Re	-3.747	3.638	-7.590	-1.030	.314
	(ln Re)^2	.159	.144	8.090	1.104	.281
	(Dx/D)*((H-Hc)/D)	-.095	1.073	-.037	-.089	.930
	(Dx/D)*(Hc/D)	.055	.716	.033	.077	.939
	(Dx/D)*((ab)0.5/D)	-6.733	6.130	-.459	-1.098	.284
	(Dx/D)*(ln Re)	-.221	.460	-.298	-.479	.636
	((H-Hc)/D)*(Hc/D)	-.049	.072	-.201	-.691	.496
	((H-Hc)/D)*((ab)0.5/D)	-2.563	.613	-1.161	-4.182	.000
	((H-Hc)/D)*(ln Re)	-.102	.046	-1.176	-2.211	.038
	((Hc)/D)*((ab)0.5/D)	.505	.409	.368	1.236	.230
	(Hc/D)*(ln Re)	-.025	.031	-.444	-.818	.422
	((ab)0.5/D)*(ln Re)	.543	.263	1.104	2.066	.051

Figure D.2: Results of the multiple regression performed with software SPSS showing the regression coefficients, standard error, standardized coefficient, t-value and significance (p-value).

D.2   Residuals statistics

A residual is the difference between the estimated model and the actual measured value. In figure D.3 one can see the predicted value maximum and minimum and the error from the measured value and the standard deviation.

Residuals Statistics[a]

	Minimum	Maximum	Mean	Std. Deviation	N
Predicted Value	1.00029	4.71042	2.67895	.977878	43
Residual	-1.274045	1.499728	.000000	.439434	43
Std. Predicted Value	-1.717	2.077	.000	1.000	43
Std. Residual	-2.098	2.470	.000	.724	43

a. Dependent Variable: Ln/D

Figure D.3: Residuals statistics from the multiple regression performed with software SPSS.

Bibliography

[1] A. C. Hoffmann and L. E. Stein, *Gas Cyclones and Swirl Tubesv.* Springer, 2008. 1.1, 1.3, 2.1.1, 2.1, 2.1, 2.2, 2.1.1, 2.3, 2.1.1, 2.1.1, 2.1.1, 2.1.2, 2.9, 2.11, 2.1.2, 2.1.2, 2.13, 2.1.3, 2.1.6, 2.1.7, 2.1.8, 2.2.1

[2] Z. L. Ji, X. L. Wu, and M. X. Shi, "Experimental research on the natural turning length in the cyclone," in *Proceedings of Filtech Europa 91 Conference*, vol. 2, pp. 583–589, Karlsruhe, 1991. 1.3.1, 2.1.7, 3.1.3

[3] A. C. Hoffmann, R. de Jonge, H. Arends, and C. Hanrats, "Evidence of the natural vortex length and its effect on the separation efficiency of gas cyclones," *Filtration and Separation*, vol. 32, no. 8, pp. 799 – 804, 1995. 1.3.1, 2.1.1, 2.1.7, 2.1.8, 3.1.4, 6.2.1, 7.7, 7.2.2, 7.3

[4] A. Gil, C. Cortès, L. M. Romeo, and J. Velilla, "Gas-particle flow inside cyclone diplegs with pneumatic extraction," *Powder Technology*, vol. 128, no. 1, pp. 78–91, 2002. 1.3.1, 2.1.1

[5] A. C. Hoffmann, W. Peng, H. W. A. Dries, M. A. Regelink, and L. E. Stein, "Experimental study of the vortex end in centrifugal separators: The nature of the vortex end," *Chemical Engineering Science*, pp. 19–28, 2005. 1.3.1, 2.1.7, 3.1.5, 7.1.1, 8.2

[6] R. M. Alexander, "Fundamentals of cyclone design and operation," *Proceedings of the Australian Institute of Minerals and Metals*, no. 152/153, pp. 202–228, 1949. 1.3.1, 2.1.7, 3.1.1

[7] H. S. Bryant, R. W. Silverman, and F. A. ZENZ, "How dust in gas affects cyclone presssure-drop," *Hydrocarbon Processing*, vol. 62, no. 6, pp. 87–90, 1983. 1.3.1, 2.1.7, 3.1.2

[8] F. P. Qian and M. Y. Zhang, "Study of the natural vortex length of a cyclone with response surface methodology," *Computers & Chemical engineering*, vol. 29, no. 10, pp. 2155–2162, 2005. 1.3.1, 2.1.7, 3.1.6, 6.2.2, 7.2.2, 7.2.2

[9] F. Kaya, I. Karagoz, and A. Avci, "Effects of Surface Roughness on the Performance of Tangential Inlet Cyclone Separators," *Aerosol science and technology*, vol. 45, no. 8, pp. 988–995, 2011. 1.3.1, 2.1.8

[10] G. I. Pisarev, T. Rødland, and A. C. Hoffmann, "Effect of wall roughness on the "end of the vortex" phenomenon in cyclone type separators," *In print*, 2011. 1.3.1, 2.1.8, 3.1.7, 6.2.3, 7.2.3

[11] A. A. Kulkarni, V. V. Ranade, R. Rajeev, and S. B. Kognati, "CFD simulation of flow in vortex diodes," *Aiche Journal*, vol. 54, pp. 1139–1152, 2008. 1.3.1

[12] J. H. Ferziger and M. Peric, *Computational Methods for Fluid Dynamics*. Springer, 3rd ed., 2002. 1.4, 2.2.2, 2.2.2, 2.2.2, 2.2.2, 2.2.2, 2.2.3, 2.2.3, 2.2.3, 2.2.3, 2.2.4

[13] R. B. Bird, W. E. Stewart, and E. N. Lightfoot, *Transport Phenomena*. Wiley, 2nd ed., 2007. 1.4

[14] G. I. Pisarev, A. C. Hoffmann, W. Peng, and H. A. Dijkstra, "Large Eddy Simulation of the vortex end in reverse-flow centrifugal separators," *Appleid mathematics and computation*, vol. 217, no. 11, pp. 5016–5022, 2011. 1.5, 2.1.1, 2.4, 6.2.2

[15] V. Gjerde, "The Natural Vortex Length in Centrifugal Separators," Master's thesis, Depertment of Physics and Technology, University of Bergen, 2010. 1.5, 2.1.5, 3.1.7, 4.0.4, 7.1.1

[16] T. Rødland, "Experimental and Theoretical Study on the Effect of Wall Roughness on the phenomenon "End of the Vortex" in Swirl Tubes," Master's thesis, Depertment of Physics and Technology, University of Bergen, 2011. 1.5, 2.1.8, 3.1.7, 6.2.3, 7.2.3

[17] D. W. Green and R. H. Perry, *Perry's chemical engineers' handbook*. McGraw - Hill, 8 ed., 2007. 2.1.1

[18] B. Zhao, Y. Su, and J. Zhang, "Simulation of gas flow pattern and separation efficiency in cyclone with conventional single and spiral double inlet configuration," *Chemical engineering research & Design*, vol. 84, no. A12, pp. 1158–1165, 2006. 2.1.1, 2.3

[19] F. Qian, J. Zhang, and M. Zhang, "Effects of prolonged vertical tube on the separation performance of a cyclone," *Journal of Hazardous Materials*, no. B136, pp. 822–829, 2006. 2.1.1

[20] D. C. Wilcox, *Turbulence Modeling for CFD*. DCW Industries, 2 ed., 1998. 2.1.2, 2.1.2, 2.1.2, 2.8, 2.2.1, 2.2.2, 2.2.2, 2.2.2, 2.2.2, 2.2.3, 2.2.3

[21] W. L. McCabe, J. C. Smith, and P. Harriott, *Unit operations of chemical engineering*. Mcgraw-Hill, 7 ed., 2005. 2.1.2, 2.1.2, 2.1.2, 2.1.2, 2.1.8

[22] A. N. Kolmogorov, "Local structure of Turbulence in Incompressible Viscous Fluid for Very Large Reynolds Number," *Doklady Akademiya Nauk SSSr*, vol. 30, pp. 299–303, 1941. 2.1.2, 2.1.2

[23] D. C. Wilcox, *Turbulence Modeling for CFD*. DCW Industries, 2006. 2.1.2

[24] R. B. Xiang, S. H. Park, and K. W. Lee, "Effects of cone dimension on cyclone performance," *Journal of Aerosol science*, vol. 32, no. 4, pp. 549–561, 2001. 2.1.7

[25] T. G. Chuah, J. Gimbun, and T. S. Y. Choong, "A CFD study of the effect of cone dimensions on sampling aerocyclones performance and hydrodynamics," *Powder Technology*, vol. 162, no. 2, pp. 126–132, 2006. 2.1.7

[26] K. Elsayed and C. Lacor, "The effect of cyclone inlet dimensions on the flow pattern and performance," *Applied mathematical modelling*, vol. 35, no. 4, pp. 1952–1968, 2011. 2.1.7

[27] A. Raoufi, M. Shams, M. Fazaneh, and R. Ebrahimi, "Numerical simulation and optimization of fluid flow in cyclone vortex finder," *Chemical Engineering and Processing*, 2007. 2.1.7

[28] J. Meyers, B. J. Geurts, and P. Sagaut, *Quality and Reliability of Large-Eddy Simulations.* Springer, 2008. 2.2.3, 2.2.3

[29] CD-adapco, *User Guide STAR CCM+*. CD-adapco, 5.06.007 ed., 2010. 2.2.3, 5.2, 5.3, 5.3, 6.1

[30] Z. L. Ji, Z. Xiong, X. Wu, H. Chen, and H. Wu, "Experimental investigations on a cyclone separator preformance at an extremely low particle consentration," *Powder Technology*, vol. 191, pp. 254–259, 2009. 3.1.3

[31] F. Qian and Y. Wu, "Effects of the inlet section angle on the separation performance of a cyclone," *Chemical engineering research & Design*, vol. 87, pp. 1567–1572, 2009. 3.1.6

[32] F. Qian, X. Huang, and M. Zhang, "Study of Gas shortcut flow rate in cyclone with different inlet section angles using Response surface methodology," *International Journal of Chemical reaction engineering*, vol. 7, no. A30, 2009. 3.1.6

[33] G. I. Pisarev, *Experimental and numerical study of the End of the Vortex phenomenon.* PhD thesis, Univerisity of Bergen, 2011. 3.1.7

[34] W. Griffiths and F. Boysan, "Computational fluid dynamics (CFD) and empirical modelling of the performance of a number of cyclone samplers," *Journal of Aerosol Science*, vol. 27, no. 2, pp. 281 – 304, 1996. 3.2.1

[35] F. Boysan, W. H. Ayers, and J. Swithenbank, "A fundamental mathematical-modeling approach to cyclone design," *Transactions of the institution of chemical engineers*, vol. 60, no. 4, pp. 222–230, 1982. 3.2.1

[36] A. J. Hoekstra, J. J. Derksen, and H. E. A. V. D. Akker, "An experimental and numerical study of turbulent swirling flow in gas cyclones," *Chemical Engineering science*, vol. 54, no. 13-14, pp. 2055–2065, 1999. 15th International Symposium on Chemical Reaction Engineering (ISCRE 15), NEWPORT BEACH, CA, SEP 13-16, 1998. 3.2.2, 3.2.3

[37] A. J. Hoekstra, *Gas Flow field and collection efficiency of cyclone separators*. PhD thesis, Delft Technical University, 2000. 3.2.2, 6.2.2

[38] J. J. Derksen and H. E. A. V. den Akker, "Simulation of vortex core precession in a reverse-flow cyclone," *Aiche Journal*, vol. 46, no. 7, pp. 1317–1331, 2000. 3.2.3, 6.2.2

[39] J. J. Derksen, "Simulations of confined turbulent vortex flow," *Computer & Fluids*, vol. 34, no. 3, pp. 301–318, 2005. 3.2.3

[40] J. J. Derksen, H. E. A. V. den Akker, and S. Sundaresan, "Two-way coupled large-eddy simulations of the gas-solid flow in cyclone separators," *Aiche Journal*, vol. 54, no. 4, pp. 872–885, 2008. 3.2.3

[41] G. Gronald and J. J. Derksen, "Simulating turbulent swirling flow in a gas cyclone: A comparison of various modeling approaches," *Powder Technology*, vol. 205, pp. 160–171, 2011. 3.2.3

[42] G. E. P. Box, J. S. Hunter, and W. G. Hunter, *Statistics for Experimenters*. Wiley, 2nd ed., 2005. 5.1, 5.1.1, 5.1.2, 5.1, 5.1.3

[43] D. C. Montgomery, *Design and Analysis of Experiments*, vol. 6. John Wiley and Sons, inc., 2005. 5.1, 5.1.2, 5.1.3

[44] D. R. Cox and N. Reid, *The Theory of the Design of Experiments*. Chapman & Hall, 2000. 5.1.1

[45] R. E. Walpole, R. H. Myers, S. L. Myers, and K. Ye, *Probability & Statistics for Engineers & Scientists*. Pearson Education International, Prentice Hall, 2002. 5.1.1, D.1

[46] A. I. Khuri and J. A. Cornell, *Responce surfaces, Designs and analyses*. Marcel Dekker, Inc., 1987. 5.1.3, 5.1.3, 5.1

[47] G. E. P. Box and N. R. Draper, *Empirical model-building and response surfaces*. John Wiley and Sons, inc., 1987. 5.1.3, 5.1.3, 5.1

[48] R. H. Myers and D. C. Montomery, *Response surface methodology*. Wiley, 1995. 5.1.3

[49] CD-adapco, *Methodology Star-CD*. CD-adapco, 4.10 ed., 2009. 5.2

[50] M. Helbæk, *Statistikk for kjemikere*. Tapir Akademisk Forlag, 2001. D.1